UNIVERSITY OF OKLAHOMA

GRADUATE COLLEGE

USING CORRELATED IMAGING AND DIFFERENCE FREQUENCY GENERATION TO

DETERMINE THE GROUP DELAY FOR AN UNKNOWN ULTRA SHORT OPTICAL

PULSE: AN ANALYTICAL AND NUMERICAL SIMULATION CALCULATION

A DISSERTATION

SUBMITTED TO THE GRADUATE FACULTY

in partial fulfillment of the requirements for the

Degree of

ELECTRICAL AND COMPUTER ENGINEERING

By

Kyrus Kuplicki
Norman, Oklahoma
2022

USING CORRELATED IMAGING AND DIFFERENCE FREQUENCY GENERATION TO
DETERMINE THE GROUP DELAY FOR AN UNKNOWN ULTRA SHORT OPTICAL
PULSE: AN ANALYTICAL AND NUMERICAL SIMULATION CALCULATION

A DISSERTATION APPROVED FOR THE

SCHOOL OF ELECTRICAL AND COMPUTER ENGINEERING

BY THE COMMITTEE CONSISTING OF

Dr. Hazem Refai, Chair

Dr. James Sluss

Dr. Samuel Cheng

Dr. Daniel Hamlin

ACKNOWLEGMENTS

Table of Contents

List of Tables

List of Figures

Abstract

A pulse laser emits ultrashort optical pulses with pulse widths on the order of pico-seconds and narrower. A full characterization of these optical pulses requires complete knowledge of their corresponding spectral amplitude and phase. Once complete knowledge of the corresponding spectral amplitude and phase are known for a pulse it can then pass through a pulse modulator to be manipulated to nearly any desired shape. While spectral amplitude is easy to achieve, the square root of measured spectral intensity, spectral phase is unobtainable with current measuring equipment. Group delay is the derivative of spectral phase with respect to frequency. Spectral phase is the integral of group delay with respect to frequency plus a constant frequency independent phase. While group delay can be determined by the following techniques: frequency resolved optical gating (FROG), spectral phase interferometry for direct electric-field reconstruction (SPIDER), and multiphoton intrapulse interference phase scan (MIIPS) a new way of determining group delay is presented.

Determining group delay is achieved through the combination of four things: difference frequency generation in a nonlinear material, a frequency to spatial conversion, a binary spatial light modulator (BSLM), and correlated imaging (aka ghost imaging). A newly generated frequency due to difference frequency generation has a phase that is a result of an integral sum of phase differences. This phase can be determined as a result of frequency down shift due to difference frequency generation. Correlated imaging uses two detectors: one detector spatially resolves an incident field upon an object while the other detector which has no spatial resolution

measures the fields response to the object. An image of the object is formed through the cross correlation of the two detectors involving many different realizations. By using a frequency to spatial conversion and BSLM we can select which frequencies contribute to the integral sum of phase differences. By correlating the contributing frequencies to the resulting phase of the newly generated frequency through many different BSLM realizations group delay can be determined. Group delay is shown to be able to be determined this way through analytical calculations and numerical simulation.

Chapter 1

1. Introduction

With the advent of the Laser (light amplification by stimulated emission) in 1960 [1-3], it has been said and come true that there are countless uses for the laser. While there are many lasers used in countless various ways there are two main types of lasers: continuous [4] and pulsed [1,5]. A continuous laser emits light at a constant intensity as a function of time. Some common examples of a continuous laser include: a laser pointer, the commonly used helium-neon (HeNe) laser, and the read/write laser used on a cd drive. Unlike the continuous laser, a pulsed laser only delivers field/photons of light over a small spatiotemporal window. The most common pulsed laser is a mode locked laser. One of the first pulsed lasers was a Nd:Glass laser [5] developed in 1965 which had a pulse duration of 10 picoseconds. Research into decreasing pulse duration for various laser types was not until the late 70's and throughout the 80's. During this time, pulse duration was decreased from the tens of picoseconds with the mode-locked diode laser [6-8] to the hundredths of picoseconds with CPM Ring Dye laser [9,10] and pulse compression [11-13]. Notably, a one picosecond pulse has a spatial length of 1/3mm, while a 100-femtosecond pulse has a spatial length of 33μm (about the diameter of a human hair). These short pulses allow for a wide range of different applications: increased data transmission, imaging on an ever decreasing temporal and spatial scale, and achieving high field densities.

As the temporal pulse duration decreases, the pulse spectral bandwidth increases. Furthermore, the corresponding spectral phase of the spectral bandwidth is also a determining

factor for the pulse shape and duration (both spatially and temporally). This means for a given spectral bandwidth, there are nearly an infinite number of different pulse shapes based on the corresponding spectral phase. In order to fully characterize a short pulse both quantities; spectral amplitude and spectral phase need to be known. Once these two quantities are known full control over the shape of short pulses is achievable through amplitude modulation and spectral phase modulation. While determining the spectral amplitude of a short pulse is easy, it is the square root of the measured spectral intensity, spectral phase is currently impossible to measure. Spectral phase is determined by measuring the field as a function of time and then preforming a Fourier transform to convert the time domain temporal measurement to the frequency domain. Once in the frequency domain spectral phase is achieved via the complex amplitude of each frequency. Currently there is no device that can measure the optical pulse's field as a function of time. This is because the current measurement sampling time is much greater than one over the frequency being measured and as such the corresponding phase information is lost. With ultrashort pulses having pulse durations on the order of picoseconds and their corresponding contributing frequencies having temporal oscillation on the order of femtoseconds, and with sampling oscilloscopes measurements of tens of picoseconds, direct determination of spectral phase is an elusive value.

Even though spectral phase is an elusive measurement, techniques have been developed to measure/determine group delay (the derivative of spectral phase with respect to frequency). The well-known current techniques used to measure/determine group delay are: frequency resolved optical gating (FROG) [14-16], spectral phase interferometry for direct electric-field reconstruction (SPIDER) [17], and multiphoton intrapulse interference phase scan (MIIPS) [18-

2

20]. Each of these stated techniques have one thing in common, they each use a nonlinear optical material to generate a new frequency by combining two frequencies. A newly created frequency generated from a nonlinear optical material can be generated in 1 of 4 ways: frequency doubling, difference frequency generation, sum frequency generation, and optical rectification. FROG and MIIPS both use frequency doubling to generate information about group delay, while SPIDER uses sum frequency generation. *This dissertation will demonstrate using difference frequency generation and Ghost Imaging to determine the group delay of an unknown optical pulse through analytical calculation and numerical simulations.*

1.1   Importance of Pulse Shaping

Pulses emitted by pulse lasers can be shaped. Gaussian pulses are the most common pulse shape, but others including square, sawtooth, circular can be generated with limited bandwidth and a known spectral amplitude.

1.1.1   Bandwidth Limited Pulse

The minimum possible pulse duration for a given spectral bandwidth is called a bandwidth-limited pulse; it is also known as a Fourier-transform-limited pulse. This specific pulse shape occurs when the spectral phase is constant across its spectral bandwidth. As stated above direct measurement of spectral phase is currently impossible for optical pulses; we must rely on group delay to determine whether the optical pulse bandwidth limited. The group delay is the derivative of the spectral phase with respect to frequency. If a group delay is equal to zero, it indicates that the corresponding spectral phase is constant. Forcing a pulse to have limited bandwidth, its spatiotemporal width is minimized for a given spectral amplitude. The minimized pulse can then be used in imaging, communications, and micro manufacturing.

In 1990 Web and Denk implemented a microscope that could cause simultaneous multiple fluorophore excitation using near-IR light pulses. This two-photon microscopy became widely used in the biomedical imaging field, because it reduced photodamage out-of-focus photobleaching and fluorescence scattering. This is achieved by the inherent instantaneous peak intensity and narrow focal plane of excitation. bandwidth limited pulses take less energy per pulse compared to a non-bandwidth limited counterpart to achieve a given intensity with reduced of light-induced damage and photobleaching [21].

Using On/Off keying modulation, optical communication presents ones with light transmissions and zeros with no light transmission. Maximum achieved data rate of an optical communication is directly proportional to receiver's ability to distinguish ones from zeros. As an optical pulse travel through a fiber, it experiences group velocity dispersion (GVD). The frequencies within the optical pulse travel at different speeds which cause the optical pulse to broaden as it travels through the fiber. Broadening optical pulses limit the data rate of a fiber. An optimal data rate occurs when bandwidth limited pulses are incident upon the receiver placed at the end of an optical fiber. To achieve an optimal data rate a chirp can be placed upon the pulse at the transmitter to compensate for the GVD that the optical pulse experiences as it travels through a fiber. Group delay is important to compensate for the broadening of pulse and determine the setting of a GVD.

Another application for bandlimited optical pulses is as electrical components become smaller over time, the machining needed to effectively use the smaller components have shrunk. Micromachining uses optical pulses to remove unwanted material [22-25]. Generally shorter pulse widths provide better spatial resolution, depth control, and edge quality due to a minimized peripheral thermal damage. In order to remove unwanted materials, the optical pulse must have a

laser power that exceeds the material's ablation threshold power. Pulse power below the ablation threshold power is wasted energy dissipates as thermal energy, may cause deformation in the material.
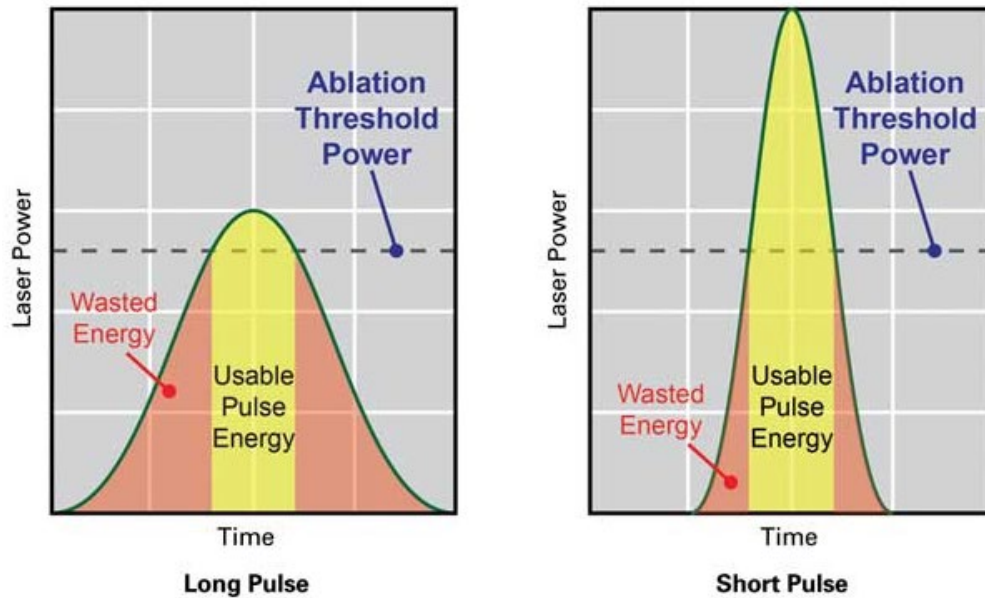
Figure 1 : Usable laser power for ablation must surpass the ablation threshold power for the material. Laser power below the ablation threshold power is wasted energy that deforms the surrounding material [26].

Bandwidth limited pulse would deliver the optimal amount of usable pulse energy emitted by the pulse laser that minimizes the potential material deformations in the heat affected zone.

This dissertation is organized as follows. I first present the mathematical foundation of light wave nature, optical pulse and its phase in chapter 2. Ghost imaging will be covered in chapter 3, while light interactions with nonlinear materials to determine the group delay for an unknown ultrashort pulse are presented in chapter 4. Chapter 5 will explain the conditions under which a group delay frequency-based ghost imaging can be used. Chapter 6 will present analytically simulated results of determining group delay for an unknown ultrashort pulse. Chapter 7 we will be look at some of the errors associated with other techniques that currently used to measure. Chapter 8 provides concluding remarks.

Chapter 2

2. Wave Nature of Light

2.1 Wave Function

To begin to understand the wave nature of light we begin by describing the wave function as $u(r,t)$ where $r = (x,y,z)$ is position and t is time. This wave function satisfies a partial differential equation called the wave equation:

$$\nabla^2 u - \frac{1}{c^2}\frac{\partial^2 u}{\partial t^2} = 0 \tag{1}$$

where c is the speed of light in the propagating material, ∇^2 is the Laplacian operator in the Cartesian coordinates $\left(\nabla^2 = \frac{\partial^2}{\partial x^2} + \frac{\partial^2}{\partial y^2} + \frac{\partial^2}{\partial z^2}\right)$. The first important thing to note is that due to the wave equation (1) being linear that the principle of superposition applies. This means if $u_1(r,t)$ and $u_2(r,t)$ are both possible solutions then $u(r,t) = u_1(r,t) + u_2(r,t)$ is also a possible solution.

2.1.1 Monochromatic Wave

The simplest light wave solution to the wave equation is a monochromatic wave with temporal and spatial dependence, which is represented by the following:

$$u(r,t) = a(r)\cos(2\pi v t + \phi(r)) \tag{2}$$

where $a(r)$ is amplitude, $\phi(r)$ is phase, and v is frequency. A representation of a monochromatic wave can be seen in figure 1.
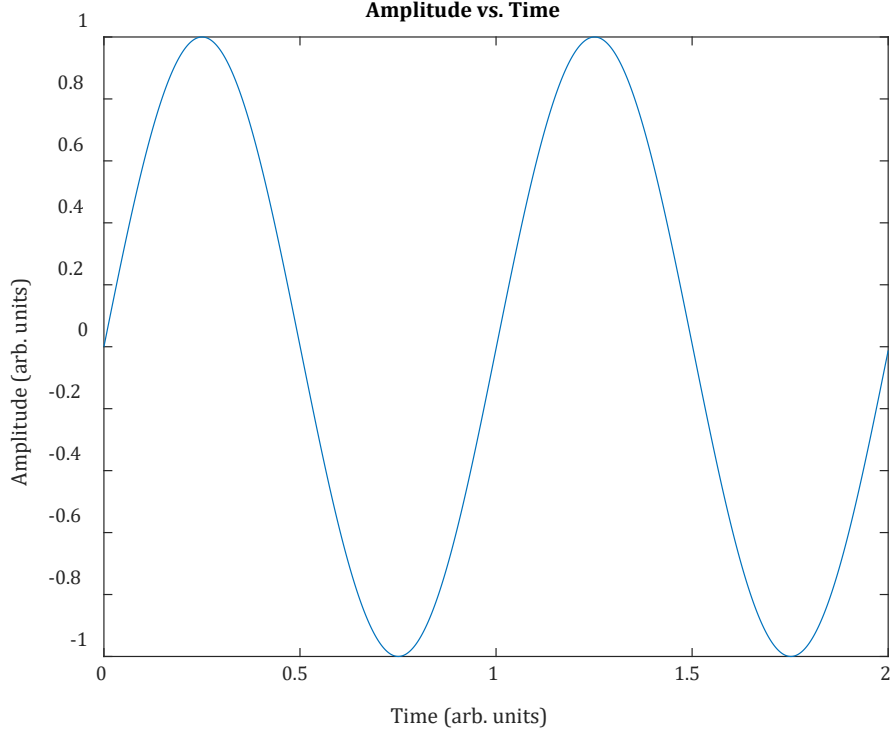
Figure 2: A monochromatic wave function with unit amplitude and frequency. The monochromatic wave function has an initial phase of $-\pi/2$ as described by equation (2).

An equally valid and sometimes more convenient way of describing a monochromatic wave is through the complex wave function.

$$U(r,t) = a(r)e^{i\phi(r)}e^{i2\pi vt} \tag{3}$$

In relation to equation (2)

$$u(r,t) = Re\{U(r,t)\} = \frac{1}{2}[U(r,t) + U^*(r,t)] \tag{4}$$

The complex wave function must satisfy the following wave equation:

$$\nabla^2 U - \frac{1}{c^2}\frac{\partial^2 U}{\partial t^2} = 0 \tag{5}$$

the complex wave function (3) can be described it in terms of its spatial dependence and its time independence as follows.

$$U(r,t) = U(r)e^{i2\pi vt} \tag{6}$$

7

The time independent element of equation (6) $U(r) = a(r)e^{i\phi(r)}$ is commonly referred to as the complex amplitude of the wave. The temporal independence and dependence of this can be seen in parts a and b of figure 2.
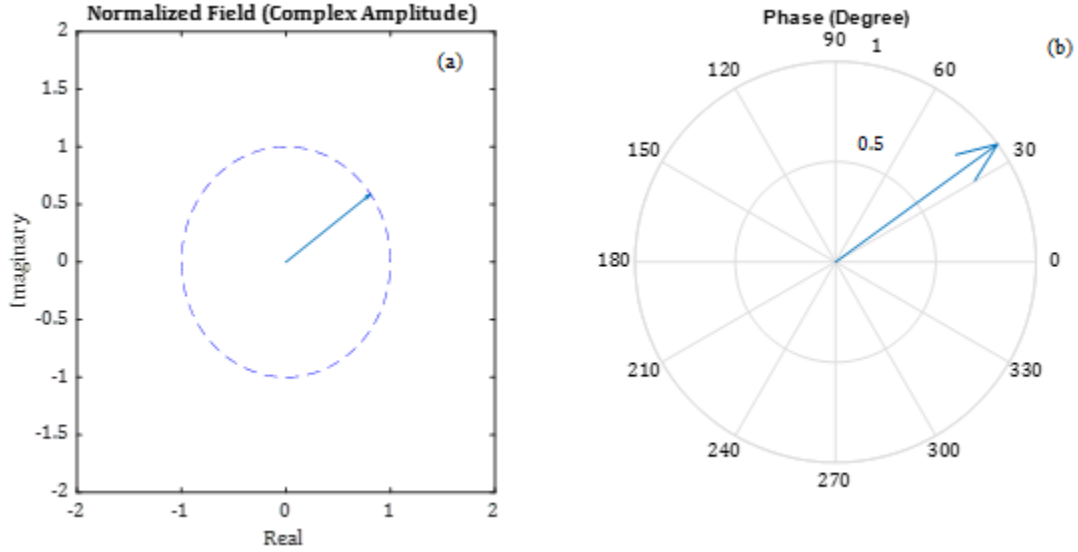
Figure 3: Given a position r in figure 2(b) the magnitude $|U(r)| = a(r)$ is the amplitude of the wave with $\phi(r)$ being its phase. Figure 2(a) shows the temporal dependence of the complex wave function by a phasor that rotates with angular velocity $\omega = 2\pi v$.

Now by inserting equation (6) into the complex wave function (5), one will come up with Helmholtz equation:

$$\nabla^2 U + k^2 U = 0 \qquad (7)$$

which introduces the wave number (k) with it being:

$$k = \frac{2\pi v}{c} = \frac{\omega}{c} \qquad (8)$$

The wave number may not seem relevant now, but its relevance will be clear in the generation of a new wave with frequency c from two waves with frequencies a and b where $c \neq a \; or \; b$.

Now since the frequencies of an optical field are typically much higher when compared to the sampling rate of a measuring device, we measure optical intensity, which is defined as the

optical power per unit area, and not field strength. Optical intensity is proportional to the average

of the squared wave function.

$$I(r,t) = 2\langle u^2(r,t) \rangle \tag{9}$$

For a monochromatic wave, its intensity is the absolute square of its complex amplitude. This can

be clear by inserting equation (2) into equation (9).

$$2u^2(r,t) = a^2(r) \cos^2\big(2\pi\pi vt + \phi(r)\big) \tag{10}$$

$$= |U(r,t)|^2\{1 + \cos(2[2\pi\pi vt + \phi(r)])\} \tag{11}$$

When the measurement time much greater than the optical period of $1/v$, the second term in

equation (11) disappears, therefore one is left with:

$$I(r,t) = |U(r,t)|^2 \tag{12}$$

2.1.2 Plane Wave

The number of wavefunctions that can satisfy the Helmholtz wave equation are numerous.

Many of the wavefunctions are quite complex and they present many mathematically challenging

problems. Thankfully, superposition still applies to the Helmholtz equation and as such many

various complex wavefunctions can be treated through a plane wave approximation. The plane

wave approximation is akin to taking the Taylor series of a complex function. The Taylor series

is an infinite sum of ever-increasing power of polynomials that approximate a complex function

$f(x)$. The accuracy of the series increases with the addition of higher-degree polynomials

provided that the approximation takes place within the interval of convergence. Outside this

interval of convergence, the complex function cannot be accurately approximated regardless of the

degree the polynomial approximation is taken to. Unlike the Taylor series the plane wave

approximation does not have a limited interval of convergence with respect to approximating

complex wave functions. A plane wave, which is a solution to the Helmholtz equation has a complex amplitude of:

$$U(r) = Ae^{i\bar{k}r} = Ae^{i(k_x x + k_y y + k_z z)} \tag{13}$$

where A is a constant called the complex envelope and $\bar{k} = (k_x, k_y, k_z)$ is called the wave vector. The magnitude of the wave vector $k_x^2 + k_y^2 + k_z^2 = k^2$ is the wavenumber k noted in equations (7) and 8. The purpose of wavenumber k is that it depicts the travel direction of the wavefunction. The travel direction of wave function corresponds to the spatial planes with constant phase, also called wavefronts. The phase of a given spatial plane is $arg\{U(r)\} = arg\{A\} - \bar{k} \cdot r$. The corresponding spatial plane with the same phase occur with $\bar{k} \cdot r = k_x x + k_y y + k_z z = 2\pi q + arg\{A\}$ where q is an integer. Consecutive spatial planes with the same phase are separated by a distance of $\lambda = \frac{2\pi}{k}$. This is referred to as a frequency's corresponding wavelength.

$$\lambda = \frac{c}{v} \tag{14}$$

Now taking the travel direction along the z-axis with $U(r) = Ae^{-ikz}$ corresponds to a wavefunction of equation (15):

$$u(r, t) = |A| \cos[2\pi vt - kz + arg\{A\}]$$

$$= |A| \cos\left[2\pi v\left(t - \frac{z}{c}\right) + arg\{A\}\right] = |A| \cos[\omega(t - kz) + arg\{A\}] \tag{15}$$

This wavefunction is periodic in time with a period of $1/v$ and periodic in space with a period of $2\pi/k$. The wave phase varies as function in both time and space; the variables $(t - z/c)$ is called the phase velocity of the wave. Likewise, we can also view the phase velocity $(t - kz)$ in relation to angular frequency ω using equation (8).

Until this point, we have assumed that the waves are traveling in free space. When light waves travel through a medium it interacts with the medium, slowing its travel speed among others. This reduction in speed is proportional to the mediums refractive index n.

$$c = \frac{c_0}{n} \tag{16}$$

This refractive index also affects the wavelength in the medium $\lambda = c/v = c_0/nv$ so $\lambda = \lambda_0/n$ where λ_0 is the wavelength in free space. This in turn affects the wavenumber k. It is increased by a factor equal to the index of refraction $k = 2\pi/\lambda = 2\pi n/\lambda_0$. When a monochromatic light plane wave travels through a medium with refractive index n, the velocity, wavelength, and wavenumber change except its frequency that remains constant with respect to traveling in free space.

$$c = \frac{c_0}{n} \tag{17}$$

$$\lambda = \frac{\lambda_0}{n} \tag{18}$$

$$k = nk_0 \tag{19}$$

This is not true when light travels though non-linear materials; new frequencies will be generated.

2.1.3 Fourier Transform

Previously, we have established a mathematical representation for a monochromatic wave and a monochromatic plane wave. These monochromatic waves extend over all time and space of a 2D plane and they constitute an ideal light wave. An actual optical pulse is of a finite spatial space and temporal duration. To construct an optical pulse, we can use the principle of superposition with many different monochromatic waves. We will be applying the Fourier method to deconstruct an arbitrary optical pulse d $u(t)$ into a superposition of harmonic functions of

different frequencies each of which have an associated amplitude and phase. Taking a sum of monochromatic waves to infinitum we get an integral sum of all frequencies, amplitudes, and phases which is:

$$u(t) = \int_{-\infty}^{\infty} u(v)e^{i2\pi vt}dv \tag{20}$$

$u(v)$ can be determined by carrying out the Fourier transform

$$u(v) = \int_{-\infty}^{\infty} u(t)e^{-i2\pi vt}dt \tag{21}$$

Equations (20) and (21) represent a Fourier transform pair. If either the functions $u(t)$ or $u(v)$ is known, the other can be determined through a Fourier transform. In this case a complex-valued temporal function $u(t)$ is decomposed into a superposition integral of harmonic functions of different frequencies (v) and complex amplitudes. Both functions $u(t)$ and $u(v)$ are equivalent in what they represent. $u(t)$ is the time-domain representation, while $u(v)$ is the frequency-domain representation. One way to realize their equivalence is through the conservation of energy. This is done through Parseval's Theorem which states that the signal energy, which is the integral of the signal power $|u(t)|^2$, equals the integral of the energy spectral density $|u(v)|^2$.

$$\int_{-\infty}^{\infty} |u(t)|^2 dt = \int_{-\infty}^{\infty} |u(v)|^2 dv \tag{22}$$

The Fourier transform has many other properties aside from Parseval's Theorem. This dissertation requires three important properties: linearity, convolution, and symmetry theorems.

$\quad$ <u>Linearity:</u> $F[u_1(t) + u_2(t)] = F[u_1(t)] + F[u_2(t)]$ The Fourier transform of a weighted sum (of two or more functions) is equal to the sum of the individual weighted functions Fourier transforms.

Symmetry: If $u(t)$ is real then $u(v)$ has Hermitian symmetry $u(-v) = u^*(v)$. Symmetry also states that if $u(t)$ is real and symmetric $u(v)$ is also real and symmetric.

Convolution Theorem: If the Fourier transform of $u_1(t)$ and $u_2(t)$ are $u_1(v)$ and $u_2(v)$ respectively, then the Fourier transform of their product

$$u_3(v) = u_1(v)u_2(v) \tag{23}$$

is

$$u_3(t) = \int_{-\infty}^{\infty} u_1(t) * u_2(t - \tau)d\tau \tag{24}$$

Equation (24) is known as a convolution in the time domain between the two functions $u_1(t)$ and $u_2(t)$. The convolution theorem simply states that a convolution in one domain is equivalent to a multiplication in another domain, if the two domains constitute a Fourier transform pair.

2.1.4 Polychromatic wave/Pulsed Light

Equation (20) extends over both positive and negative frequencies. It is known that the optical temporal pulse $(u(t))$ in equation (20) is real which means that, $u(-v) = u^*(v)$, by using the symmetry rule of a Fourier transform. This means that negative frequency components are not actually independent from the positive frequency components but are rather conjugated versions of the corresponding positive-frequency components. Knowing this fact, it is at times convenient to represent the real temporal function $u(t)$ by using only the positive frequencies as seen in the following complex function:

$$U(t) = 2\int_0^{\infty} u(v)e^{i2\pi vt}dv = 2\int_0^{\infty} A(v)e^{i2\pi vt+\phi(v)}dv \tag{25}$$

Equation (25) includes only the positive valued frequency components (which are multiplied by a factor of 2), while negative frequencies are suppressed. The function of $U(t)$ has a Fourier

transform and is $U(v) = 2u(v)$ for $v \geq 0$ and 0 for $v < 0$. If the complex representation $(U(t))$ is known and the real function $u(t)$ is desired it can be determined by taking the real part of the complex function.

$$u(t) = Re\{U(t)\} = \frac{1}{2}[U(t) + U^*(t)] \tag{26}$$

A simple and useful example of this complex representation is that of a real harmonic function $u(t) = A\left(\frac{\omega}{2\pi}\right) \cos\left(\omega t + \phi\left(\frac{\omega}{2\pi}\right)\right)$. It is used to describe a monochromatic wave in a complex harmonic function $U(t) = 2A\left(\frac{\omega}{2\pi}\right) e^{i\omega t + \phi\left(\frac{\omega}{2\pi}\right)}$. Through this representation a polychromatic wave is described by the superposition of complex representations of each of its monochromatic Fourier components.
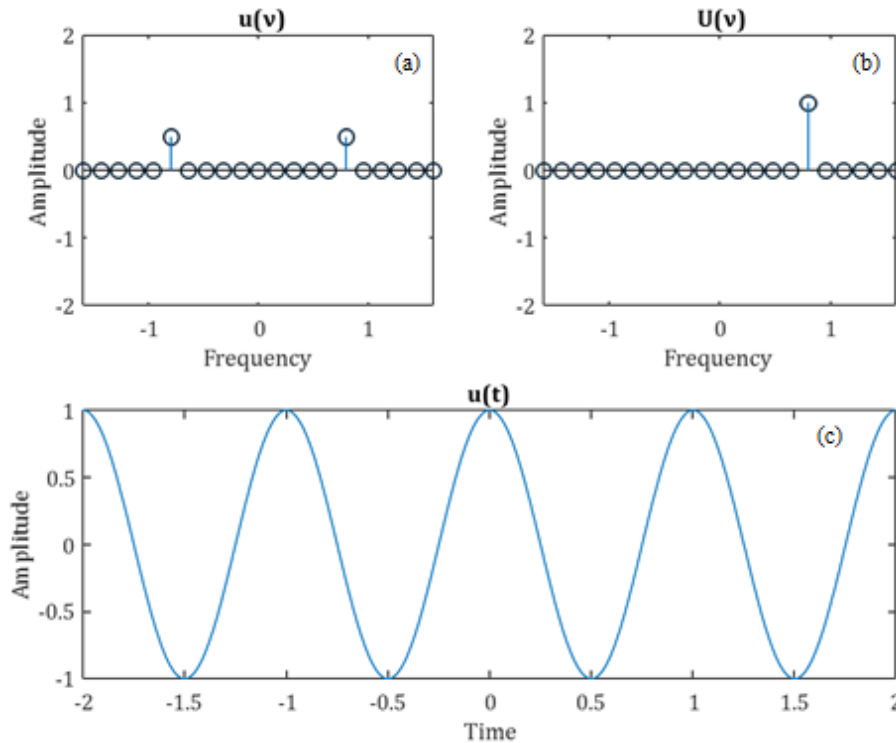
Figure 4: The time domain representation of a monochromatic wave function with unit amplitude is displayed in figure 3(c) while its frequency domain representation is seen in figure 3(a) and 3(b). The frequency domain representation seen in figure 3(a) encompasses both positive and negative frequencies using equation (21) while figure 3(b) only encompasses the positive frequencies using the Hermitian symmetry property along with equations (25) and (26).

With a polychromatic wave being the superposition of infinitely many monochromatic waves, two polychromatic waves are differentiated from one another by their corresponding complex amplitudes as a function of frequency. The complex amplitude can further be broken down into two components: maximum amplitude $A(v)$ (called spectral amplitude) and spectral phase $\phi(v)$. Both the spectral amplitude and spectral phase impact the temporal amplitude and temporal width of the polychromatic wave. For a given spectral amplitude, the minimum temporal width (a bandwidth-limited pulse) is achieved when its corresponding spectral phase is constant [27]. A polychromatic wave with a constant spectral phase has a constant group delay equal to zero. Group delay is defined as the derivative of spectral phase with respect to frequency.

$$\tau_g(\varpi) = -\frac{d\phi(v)}{dv} \tag{27}$$

Likewise knowing the group delay of a polychromatic wave, its spectral phase is the integral of group delay plus a constant phase term across the spectrum.

$$\phi(v) = \int T_g(\varpi)d\varpi + \phi(0) \tag{28}$$

As stated, polychromatic wave is a superposition of infinitely many monochromatic waves. A complete description of a wave's content is given by its spectral amplitude and its spectral phase. Further, the spectral amplitude and group delay of a polychromatic wave contains the same amount of information minus a constant phase across the spectrum. While it is easy to determine the spectral amplitude for any pulse (the square root of spectral intensity, as shown in equations (10-12), it is difficult to determine the spectral phase when sampling time is greater than a period of $1/v$. *Lack of information on spectral phase for ultra-short pulses drove the development of*

inventive ways (FROG, SPIDER, MIIPS) to determine group delay. This dissertation will describe

how to use correlated imaging in conjunction with difference frequency generation to determine

the group delay of an ultra-short pulse.

2.2 Nonlinear Light

In the previous section a basic mathematical foundation was laid out for the description of both

a monochromatic wave and the construction of a polychromatic pulse. In this section, we present

the work of Boyd [28]. The mathematical foundation for a light wave (electromagnetic radiation)

traveling through a medium is described. Specifically, we will focus on nonlinear susceptibility of

a medium to generate a new frequency from two or more monochromatic wave sources traveling

through it. We will then follow the work of Gallot and Grischkowsky [29] that expand the work

to study new frequencies generated by polychromatic sources. We must first start off with

Maxwell's equations that govern the electric and magnetic fields:

$$\nabla \times E = -\frac{1}{c}\frac{\partial B}{\partial t} \tag{29}$$

$$\nabla \times B = \frac{1}{c}\frac{\partial E}{\partial t} + \frac{4\pi}{c}J \tag{30}$$

$$\nabla \cdot E = 4\pi\rho \tag{31}$$

$$\nabla \cdot B = 0 \tag{32}$$

where E is an electric field, B is a magnetic field, J and ρ are the current and charge densities

respectively which are related by the charge conservation law.

$$\nabla \cdot J + \frac{\partial \rho}{\partial t} = 0 \tag{33}$$

Where J and ρ can be expanded into a series of multipoles [30]:

16

$$J = J_0 + \frac{\partial P}{\partial t} + c\nabla \times M + \frac{\partial}{\partial t}(\nabla \cdot Q) + \cdots \tag{34}$$

$$\rho = \rho_0 - \nabla \cdot P - \nabla(\nabla \cdot Q) + \cdots \tag{35}$$

Where P, M, and Q are the electric polarization, the magnetization, and the electric quadrupole polarization, respectively. Higher terms in this expansion contain the contributions to the magnetization and electric polarization of an increasing number of poles. In the region of optics, it has been pointed out by Landau and Lifshitz [31] that it is not meaningful to include the higher order multipoles of J and ρ terms, because the typical definitions of multipoles are unphysical. This leads us to use a generalized electric polarization P defined by:

$$J = J_{dc} + \frac{\partial P}{\partial t} \tag{36}$$

This changes the second equation of the Maxwell's equations to

$$\nabla \times B = \frac{1}{c}\frac{\partial}{\partial t}(E + 4\pi P) + \frac{4\pi}{c}J_{dc} \tag{37}$$

If it is assumed that an electric field propagating in a medium does not have a dc current running through it, the following equation describes how the electric field is affected by the medium:

$$\nabla^2\tilde{E} - \frac{n^2}{c^2}\frac{\partial^2\tilde{E}}{\partial t^2} = \frac{1}{\epsilon_0 c^2}\frac{\partial^2\tilde{P}^{NL}}{\partial t^2} \tag{38}$$

where $\tilde{P}$ is a time-varying source term that describes the mediums response to the electric field. If we take an anharmonic oscillator model approach to describe the mediums response $(\tilde{P})$ the response can be broken down/expanded into a power series of $\tilde{E}(t)$ that includes all nonlinear contributions.

$$\tilde{P}^{NL}(t) = \epsilon_0\left[\chi^{(1)}\tilde{E}(t) + \chi^{(2)}\tilde{E}^2(t) + \chi^{(3)}\tilde{E}^3(t) + \cdots\right] \tag{39}$$

$$\tilde{P}^{NL}(t) = \tilde{P}^1(t) + \tilde{P}^2(t) + \tilde{P}^3(t) + \cdots \tag{40}$$

The constants $\chi^{(i)}$ represent the nth order susceptibility of the medium. The first order linear susceptibility is expressed as:

$$\tilde{P}^1(t) = \epsilon_0 \chi^{(1)} \tilde{E}(t) \tag{41}$$

Optical effects that occur from the first order of susceptibility are diffraction, reflection, refraction, absorption, and change in phase. Within the first order susceptibility, there is no and can be no frequency mixing. This also states that each frequency is independent from all other frequencies. The mixing of different frequencies to generate a new one first occurs in the second order term due to nonlinear polarization given as follows:

$$\tilde{P}^2(t) = \epsilon_0 \chi^{(2)} \tilde{E}^2(t) \tag{42}$$

When a medium has a second order susceptibility, the total electric field $\tilde{E}(t)$ becomes a superposition of two angular frequencies ω_1 and ω_2. Angular frequency was seen being related to frequency via the wave number in equation (8), $\omega = 2\pi\nu$.

$$\tilde{E}(\omega, t) = \tilde{A}_1 e^{i(k_1 z - \omega_1 t + \varphi(\omega_1))} + \tilde{A}_2 e^{i(k_2 z - \omega_2 t + \varphi(\omega_2))} + \tilde{A}_1 e^{-i(k_1 z - \omega_1 t + \varphi(\omega_1))}$$
$$+ \tilde{A}_2 e^{-i(k_2 z - \omega_2 t + \varphi(\omega_2))} \tag{43}$$

For simplicity I shall include the corresponding phase term $\varphi(\omega_j)$ within the amplitude term $\tilde{A}_j$ and as such the incident field on the nonlinear medium is expressed as:

$$\tilde{E}(\omega, t) = A_1 e^{i(k_1 z - \omega_1 t)} + A_2 e^{i(k_2 z - \omega_2 t)} + A_1^* e^{-i(k_1 z - \omega_1 t)} + A_2^* e^{-i(k_2 z - \omega_2 t)} \tag{44}$$

The induced second order nonlinear polarization is given by:

$$\tilde{P}^2(t) = \epsilon_0 \chi^{(2)} \left(A_1 e^{i(k_1 z - \omega_1 t)} + A_2 e^{i(k_2 z - \omega_2 t)} + A_1^* e^{-i(k_1 z - \omega_1 t)} + A_2^* e^{-i(k_2 z - \omega_2 t)} \right)^2 \tag{45}$$

$$\tilde{P}^2(t) = \epsilon_0 \chi^{(2)} \big[A_1^2 e^{i2(k_1 z - \omega_1 t)} + A_1^{*2} e^{-i2(k_1 z - \omega_1 t)} + 2A_1 A_1^* + A_2^2 e^{i2(k_2 z - \omega_2 t)}$$

$$+ A_2^{*2} e^{-i2(k_2 z - \omega_2 t)} + 2A_2 A_2^* + A_1 A_2 e^{i((k_1 + k_2)z - (\omega_1 + \omega_2)t)}$$

$$+ 2A_1^* A_2^* e^{-i((k_1 + k_2)z - (\omega_1 + \omega_2)t)} + A_1^* A_2 e^{i((k_2 - k_1)z - (\omega_2 - \omega_1)t)}$$

$$+ A_1 A_2^* e^{-i((k_2 - k_1)z - (\omega_2 - \omega_1)t)} \big]$$

(46)

There are 6 terms resulting from the second order polarization which can be grouped into 4 categories:

- Second harmonic generation (SHG): A doubling of the incident frequency.

$$P(2\omega_1) = \epsilon_0 \chi^{(2)} \big(A_1^2 e^{i2(k_1 z - \omega_1 t)} + A_1^{*2} e^{-i2(k_1 z - \omega_1 t)} \big) \tag{47}$$

$$P(2\omega_2) = \epsilon_0 \chi^{(2)} \big(A_2^2 e^{i2(k_2 z - \omega_2 t)} + A_2^{*2} e^{-i2(k_2 z - \omega_2 t)} \big) \tag{48}$$

- Sum frequency generation (SFG): The resulting frequency is the sum of the two incident frequencies

$$P(\omega_1 + \omega_2) = 2\epsilon_0 \chi^{(2)} \big(A_1 A_2 e^{i((k_1 + k_2)z - (\omega_1 + \omega_2)t)} + A_1^* A_2^* e^{-i((k_1 + k_2)z - (\omega_1 + \omega_2)t)} \big) \tag{49}$$

- Difference frequency generation (DFG): The resulting frequency is the difference between the two incident frequencies

$$P(\omega_2 - \omega_1) = 2\epsilon_0 \chi^{(2)} \big(A_1^* A_2 e^{i((k_2 - k_1)z - (\omega_2 - \omega_1)t)} + A_1 A_2^* e^{-i((k_2 - k_1)z - (\omega_2 - \omega_1)t)} \big) \tag{50}$$

- Optical Rectification (OR): A resulting frequency of zero

$$P(0) = 2\epsilon_0 \chi^{(2)} [2A_1 A_1^* + 2A_2 A_2^*] \tag{51}$$

2.2.1 Monochromatic source used in difference frequency generation

Four different electric fields could be generated from the mixing of two different angular frequencies when they are incident upon a second order susceptible medium. The possible field/s that could be generated are: $E_{2\omega_1}, E_{2\omega_2}, E_{\omega_1 + \omega_2}, and\ E_{\omega_2 - \omega_1}$. However, not every one of these

possible fields will be generated by every second order susceptible medium. In order to determine which if any of these fields are generated in the second order susceptible medium, we must use Maxwell's second equation in its modified form. This modified form is a coupled differential mathematical equation.

$$\nabla^2\left(E_{2\omega_1} + E_{2\omega_2} + E_{\omega_1+\omega_2} + E_{\omega_2-\omega_1}\right) - \frac{n_{\omega_2-\omega_1}^2}{c^2}\frac{\partial^2\left(E_{2\omega_1} + E_{2\omega_2} + E_{\omega_1+\omega_2} + E_{\omega_2-\omega_1}\right)}{\partial t^2}$$

$$= \frac{1}{\epsilon_0 c^2}\frac{\partial^2 \tilde{P}^{NL}}{\partial t^2}$$

(52)

For the purpose of this dissertation, we are only concerned about examining the conditions under which difference frequency generation occurs:

$$\nabla^2\left(E_{\omega_2-\omega_1}\right) - \frac{n_{\omega_2-\omega_1}^2}{c^2}\frac{\partial^2\left(E_{\omega_2-\omega_1}\right)}{\partial t^2}$$

$$= \frac{\chi^{(2)}}{c^2}\frac{\partial^2}{\partial t^2}\left[2A_1^*A_2 e^{i((k_2-k_1)z-(\omega_2-\omega_1)t)} + 2A_1A_2^* e^{-i((k_2-k_1)z-(\omega_2-\omega_1)t)}\right]$$

(53)

Not concerning with the complex conjugate part of the wave, for the moment, we have:

$$\left[\nabla^2 A_{\omega_2-\omega_1} - \frac{n_{\omega_2-\omega_1}^2}{c^2}\frac{\partial^2 A_{\omega_2-\omega_1}}{\partial t^2}\right] e^{i(k_{\omega_2-\omega_1}z-\omega_{\omega_2-\omega_1}t)}$$

$$= \frac{2\chi^{(2)}}{c^2}\frac{\partial^2}{\partial t^2}A_1^*A_2 e^{i((k_2-k_1)z-(\omega_2-\omega_1)t)}$$

(54)

Expanding the first term on the left side and taking the partial time derivative of the right side we will obtain:

$$\left[\frac{\partial^2 A_{\omega_2-\omega_1}}{\partial z^2} + 2ik_{\omega_2-\omega_1}\frac{\partial A_{\omega_2-\omega_1}}{\partial z} - k_{\omega_2-\omega_1}^2 A_{\omega_2-\omega_1} - \frac{n_{\omega_2-\omega_1}^2}{c^2}\frac{\partial^2 A_{\omega_2-\omega_1}}{\partial t^2}\right] e^{i(k_{\omega_2-\omega_1}z-\omega_{\omega_2-\omega_1}t)}$$

$$= -\frac{2\chi^{(2)}(\omega_2-\omega_1)^2}{c^2}A_1^*A_2 e^{i((k_2-k_1)z-(\omega_2-\omega_1)t)}$$

(55)

20

By taking the slowly varying envelope approximation, we can neglect the first term on the left-hand side due to its negligible value as compared to the second term of the left-hand side. Also, in taking the second partial with respect to the fourth term on the left-hand side we will obtain:

$$\left[2ik_{\omega_2-\omega_1} \frac{\partial A_{\omega_2-\omega_1}}{\partial z} - k^2_{\omega_2-\omega_1} A_{\omega_2-\omega_1} - \frac{n^2 \omega^2_{\omega_2-\omega_1}}{c^2} A_{\omega_2-\omega_1} \right] e^{i(k_{\omega_2-\omega_1}z - \omega_{\omega_2-\omega_1}t)}$$

$$= -\frac{2\chi^{(2)}(\omega_2 - \omega_1)^2}{c^2} A_1^* A_2 e^{i((k_2-k_1)z - (\omega_2-\omega_1)t)}$$

(56)

Using $k^2_{\omega_2-\omega_1} = n^2_{\omega_2-\omega_1} \omega_{\omega_2-\omega_1}/c^2$ we get:

$$2ik_{\omega_2-\omega_1} \frac{\partial A_{\omega_2-\omega_1}}{\partial z} = -\frac{2\chi^{(2)}(\omega_2 - \omega_1)^2}{c^2} A_1^* A_2 e^{i(\{(k_2-k_1)-k_{\omega_2-\omega_1}\}z)}$$

(57)

$$\frac{\partial A_{\omega_2-\omega_1}}{\partial z} = \frac{i\chi^{(2)}(\omega_2 - \omega_1)^2}{k_{\omega_2-\omega_1} c^2} A_1^* A_2 e^{i(\{(k_2-k_1)-k_{\omega_2-\omega_1}\}z)}$$

(58)

To slightly simplify the differential equation of (57), I assume that a perfect phase-matching is achieved, resulting in $(k_2 - k_1) - k_{\omega_2-\omega_1} = 0$. When preforming the above calculation for SHG and SFG, this assumption is also considered. It is primarily the phase-matching condition (nonlinear material dependent) that determines which SHG, DFG, or SFG is generated. The resulting newly generated frequency is dampened by the amount of non-zero phase matched condition. The resulting created field of the new frequency as a function of position within the nonlinear material can be expressed as follows.

$$A_{\omega_2-\omega_1}(z) = i \sqrt{\left(\frac{n_1 \omega_{\omega_2-\omega_1}}{n_{\omega_2-\omega_1} \omega_1} \right)} \frac{A_2}{|A_2|} A_1^*(0) \sinh(\kappa z)$$

(59)

where

$$\kappa^2 = \frac{\chi^{(2)^2} \omega_1^2 \omega^2_{\omega_2-\omega_1}}{k_1 k_{\omega_2-\omega_1} c^4} |A_2|^2$$

(60)

We have obtained a new angular frequency $(\omega_2 - \omega_1)$ due to a nonlinear material from two monochromatic sources with angular frequencies ω_1 and ω_2. The initial phase of this new generated angular frequency depends on the phase of the two source frequencies. It can be found within the complex amplitude terms $A_2 A_1^*$ in equation (59). The initial phase for the newly generated frequency is the phase difference between the two source frequencies. Thus, the newly generated monochromatic field of angular frequency $(\omega_2 - \omega_1)$ has an initial phase of $\big(\varphi(\omega_2) - \varphi(\omega_1)\big)$.

2.2.2 Polychromatic sources used in difference frequency generation

I would like to now ask the question what is the initial phase for a newly generated monochromatic field if there are more than two source frequencies? To answer this question, I shall expand the source frequencies from two monochromatic fields to a polychromatic source incident upon a second order susceptible medium that will generate angular frequency (ω_k) from all possible angular frequency combinations of $(\omega_i - \omega_j)$.

$$\omega_k = \omega_i - \omega_j \tag{61}$$

The initial phase of newly generated frequency (ω_k) will have contributions from all possible frequency combinations of $(\omega_i - \omega_j)$. We will follow the work of Gallot and Grischkowsky [29] to expand to near infinitum number of source frequencies that generate a near infinitum number of difference frequency fields.

We start by first defining the polychromatic input fields:

Field 1:

$$E_1(z, \omega_1) = E_1(z, \omega_1)\hat{u}_k \tag{62}$$

$$E_1(z, \omega_1) = A_1(z, \omega_1 - \omega_0)e^{i(k_1(\omega_1)z - (\omega_1 - \omega_0)t)}$$

$$E_1(z, t) = \int_{-\infty}^{\infty} E_1(z, \omega_1 - \omega_0)d\omega_1 \tag{63}$$

Field 2:

$$E_2(z, \omega_2) = E_2(z, \omega_2)\hat{u}_k \tag{64}$$

$$E_2(z, \omega_2) = A_2(z, \omega_2 - \omega_0)e^{i(k_2(\omega_2)z - (\omega_2 - \omega_0)t)}$$

$$E_2(z, t) = \int_{-\infty}^{\infty} E_2(z, \omega_2 - \omega_0)d\omega_2 \tag{65}$$

The generated difference-frequency polychromatic field is:

$$E_3(z, \omega_3) = E_3(z, \omega_3)\hat{u}_k \tag{66}$$

$$E_3(z, \omega_3) = A_3(z, \omega_3 - \omega_0)e^{i(k_3(\omega_3)z - (\omega_3 - \omega_0)t)}$$

$$E_3(z, t) = \int_{-\infty}^{\infty} E_3(z, \omega_3 - \omega_0)d\omega_3 \tag{67}$$

With a Difference frequency of: $\omega_3 = \omega_2 - \omega_1$

With the addition of absorption, the wave vector k becomes

$$k = k' + i\beta \tag{68}$$

The polarization generation for the difference frequency:

$$P^{(2)}(\omega_3) = p^{(2)}e^{i[(k_2 - k_1)z - \omega_3 t]}\hat{u} = \chi_{ijk}^{(2)}E_1^*(\omega_1)E_2(\omega_2)\hat{u}$$

$$P^{(2)}(\omega_3) = p^{(2)}e^{i[(k_2 - k_1)z - \omega_3 t]}\hat{u} = \chi_{ijk}^{(2)}E_1^*(\omega_1)E_2(\omega_2)\hat{u} \tag{69}$$

where $\hat{u}$ is a generalized unit vector of $\hat{u}_x, \hat{u}_y, or \hat{u}_z$. Using the slowly varying amplitude

approximation for the two fields, the generated difference frequency field is:

$$\left[\frac{\partial}{\partial z} + \beta_3(\omega_3)\right]A_3(z, \omega_3 - \omega_0) = i\frac{2\pi\omega_3^2}{c^2 k_3(\omega_3)}p^{(2)}e^{(i\Delta k - [\beta_1(\omega_1) + \beta_2(\omega_2)])z} \tag{70}$$

The phase match condition is:

$$\Delta k = -k_3(\omega_2 - \omega_1) - k_1(\omega_1) + k_2(\omega_2) \tag{71}$$

The solution to the differential equation (70) is:

$$A_3(l, \omega_3 - \omega_0) = i \frac{2\pi\omega_3^2}{c^2 k_3(\omega_3)} p^{(2)} \frac{e^{(i\Delta k - [\beta_1(\omega_1) + \beta_2(\omega_2)])l} - e^{-\beta_3(\omega_3)l}}{i\Delta k - [\beta_1(\omega_1) + \beta_2(\omega_2) - \beta_3(\omega_3)]} \tag{72}$$

Using the polarization generation for the difference frequency equation, one can rewrite the previous equation to:

$$A_3(l, \omega_3 - \omega_0) = i \frac{2\pi\omega_3^2}{c^2 k_3(\omega_3)} \chi_{ijk}^{(2)}(\omega_3) \frac{e^{i\Delta kl} - 1}{i\Delta k} e^{-\beta_3(\omega_3)l} A_1^*(\omega_1 - \omega_0) A_2(\omega_2 - \omega_0) \tag{73}$$

The complex phase mismatch and absorption are expressed as:

$$\Delta k = -k_3(\omega_2 - \omega_1) - k_1(\omega_1) + k_2(\omega_2) \tag{74}$$

The total generated field for a given frequency (ω) which is created through difference frequency generation with an optical pulse within a second order susceptible medium is obtained by integration over the entire optical pulse bandwidth. To calculate this, we describe ω_1 and ω_2 as:

$$\omega_1 = \Omega \tag{75}$$

$$\omega_2 = \omega + \Omega \tag{76}$$

The total generated field becomes:

$$E_3(l, \omega) = i \int_{-\infty}^{\infty} \frac{2\pi\omega^2}{c^2 k_3(\omega)} \chi_{ijk}^{(2)}(\omega; \Omega, \omega + \Omega) \frac{e^{i\Delta kl} - 1}{i\Delta k} e^{-k_3(\omega)l} A_1^*(\Omega - \omega_0) e^{i(\Omega - \omega_0)t} A_2(\omega + \Omega$$

$$- \omega_0) e^{i(\omega + \Omega - \omega_0)t} d\Omega$$

$$E_3(l, \omega) = i \Bigg\{ \int_{-\infty}^{\infty} \frac{2\pi\omega^2}{c^2 k_3(\omega)} \chi_{ijk}^{(2)}(\omega; \Omega, \omega + \Omega) \frac{e^{i\Delta kl} - 1}{i\Delta k} A_1^*(\Omega - \omega_0) A_2(\omega + \Omega$$

(77)

$$- \omega_0) d\Omega \Bigg\} e^{-[k_3(\omega)l - \omega]t}$$

Similar to the case of two monochromatic source fields, the phase for a given angular frequency (ω) is an integral sum over the entire optical pulse with a frequency difference of $[\omega_2 - \omega_1]$ where $\omega_2 > \omega_1$ as seen in the complex amplitude terms of $A_2(\omega + \Omega - \omega_0)$ and $A_1^*(\Omega - \omega_0)$. While the above is for a given generated frequency the resulting field in the temporal domain is:

$$E_{sum}(l, t) = \int_{-\infty}^{\infty} d\omega \left[i \Bigg\{ \int_{-\infty}^{\infty} \frac{2\pi\omega^2}{c^2 k_3(\omega)} \chi_{ijk}^{(2)}(\omega; \Omega, \omega + \Omega) \frac{e^{i\Delta kl} - 1}{i\Delta k} A_1^*(\Omega - \omega_0) A_2(\omega + \Omega \right.$$

(78)

$$\left. - \omega_0) d\Omega \Bigg\} e^{-[k_3(\omega)l - \omega]t} \right] e^{-i\omega t}$$

Each angular frequency (ω) that was generated by difference frequency generation in the newly generated field $E_3(l, t)$ is a composition of all possible frequencies within the incident optical pulse that have a frequency difference of $[\omega_2 - \omega_1 = \omega]$.

In conclusion, through the current and charge density terms in Maxwell's equations and a series of multipoles, new frequencies can be generated as a light travels a medium with at least a second order susceptibility. The potential newly generated frequencies could be grouped into four different types: frequency doubling, sum frequency generation, difference frequency generation, and optical rectification. It was found that the initial phase of the generated monochromatic wave is equal to the phase difference between the two monochromatic wave sources. This was then expanded by having a polychromatic wave source instead of two monochromatic waves. This in turn generates a polychromatic wave instead of a monochromatic wave. As it turns out that the

initial phase for a given frequency within the generated polychromatic wave is an integral sum of phase differences residing from within the polychromatic wave source. With this knowledge and using ghost imaging we can decompose the integral sum into their individual phase difference components that reside within polychromatic wave source. This is important because the individual phase difference components are effectively the group delay of the polychromatic wave source. The next few chapters develop the thesis of this dissertation. I will first review spatial ghost imaging and second apply it in the frequency domain to determine the group delay of an unknown polychromatic wave.

Chapter 3

3. Correlated Imaging (aka Ghost Imaging)

In 1995 Pittman et al. [32] first demonstrated the creation of a ghost imaging using an orthogonally polarized signal and idler beams created by a type-II phase-matched spontaneous parametric down-conversion (SPDC).
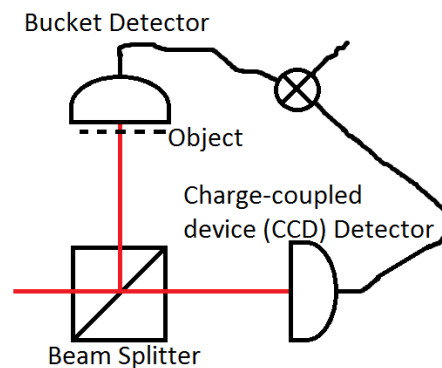
Figure 5: A simple ghost imaging setup

The entangled photon pairs created by the SPDC are separated by a polarizing beam splitter. On one leg of the setup an entangled photon interacts with the object to be imaged. The bucket detector which has no spatial resolution capabilities measures the photon count as a function of time. The leg with the charge-coupled device (CCD) detector which has spatial resolution measures the photon count as a function of time and spatial location. A ghost image is formed through a photon-coincidence count cross-correlation between the two detector measurements. A photon-coincidence is performed as opposed to a photocurrent cross correlation because of the low photon count of the SPDC. From this setup it was thought that the formation

of a ghost image relied on entanglement to generate an image. It was later demonstrated by Bennink et al. [33] in 2002 that it is possible to generate a ghost image using a pair of collimated laser beams with anti-correlated propagation directions. This sparked a debate as to if the generation of a ghost image was a classical or quantum effect [34-36]. It was determined that the generation of a ghost image produced by a classical scheme was inferior to the quantum generation of a ghost image scheme. It was when the classical scheme was expanded to a mutual coherence function with thermal light, with propagation properties similar to the biphoton quantum scheme, could generate a similar quality ghost image to the quantum scheme [37, 38]. The new classical scheme of generating a ghost image uses a laser beam that passes through a rotating ground glass diffuser to generate a time-varying optical field. This time-varying optical field is incident upon a beam splitter in where its output is used for the two legs of the classical ghost imaging scheme. From this, two competing ideas were formed about how a ghost image was generated. On the classical side we have the description of a ghost image formation based in coherence theory [39, 40] and classical statistical optics [41, 42]. On the other side we have the quantum-mechanical description of the formation of a ghost image by Scarcelli et al. [43] which was based on nonlocal two-photon interference. To unify these two competing ideas Erkmen and Shapiro formed a Gaussian-state framework that encompassed ghost images formed from both pseudothermal, biphoton, and classical phase-sensitive light [44]. Shapiro showed from the Gaussian-state framework that the biphoton-state ghost image depends on the phase-sensitive cross correlation between the two legs while the thermal-state ghost image depends on the phase-insensitive cross correlation between the two legs. Due to the fact that the formation of a ghost image is based on both phase-insensitive and -sensitive cross correlations, the ghost image generated by the biphoton scheme was not caused by quantum entanglement but by classical coherence propagation because

a Gaussian-state source can, in principle, have an arbitrary amount of phase-sensitive and - insensitive cross correlation functions.

A ghost image is formed from the cross-correlation measurements made by two detectors. These cross-correlation measurements can either be phase-sensitive or phase-insensitive. The difference between the two is the quality of the ghost image with the better one coming from the phase-sensitive cross correlation. One way of generating a field with a cross correlation is to use a speckle field [45]. To generate this speckle field one can either pass a coherent beam through a rotating ground glass [45] or by having a spatially coherent beam illuminate a spatial light modulator (SLM) that is driven by an independent random noise process [46].

3.1   Spatial Ghost Imaging

A ghost image is generated through the correlation between the spatially resolved measurements made by a spatially resolving detector and the non-spatially resolved intensity measurements made by the bucket detector placed immediately behind the object. An image of the object is created by correlating the measured intensity-intensity statistics.

$$G(x,y) = \frac{1}{N}\sum_{s=1}^{N} I_o^{(s)} I^{(s)}(x,y) \tag{79}$$

where N is the total number of samplings, $I^{(s)}(x,y)$ is the measured intensity by the reference detector and

$$I_o^{(s)} = \iint O(x',y')I^{(s)}(x',y')dx'dy' \tag{80}$$

where $I_o^{(s)}$ is the bucket detector measurement for a sampling, $O(x',y')$ is the unknown object, and $I^{(s)}(x',y')$ is the incident Intensity of the incident field.

The information about the object is contained within the cross correlation between the two intensities (I_o and I). Within the $G_{m,n}(x,y)$ term there is extraneous information. This is best seen with the Gaussian moment theorem [47]. We shall rewrite the $G_{m,n}(x,y)$ term in the form of its fields and applying the Gaussian moment theorem we have.

$$G_{m,n}(x,y) = \mathrm{E}[E_o E_o^* E_1 E_1^*] \tag{81}$$

$$\mathrm{E}[E_o E_o^* E_1 E_1^*] = \mathrm{E}[E_o E_o^*]\mathrm{E}[E_1 E_1^*] + \mathrm{E}[E_o E_1]\mathrm{E}[E_o^* E_1^*] + \mathrm{E}[E_o E_1^*]\mathrm{E}[E_o^* E_1] \tag{82}$$

The first term on the right side of the equation involves no cross correlation between the two fields. This term like the $G_{m,n}(x,y)$ term; it is a known quantity and it can be therefore subtracted from the $G_{m,n}(x,y)$ term to end up with just the cross correlation terms.

$$\mathrm{E}[E_o E_o^* E E^*] - \mathrm{E}[E_o E_o^*]\mathrm{E}[E_1 E_1^*] = \mathrm{E}[E_o E_1]\mathrm{E}[E_o^* E_1^*] + \mathrm{E}[E_o E_1^*]\mathrm{E}[E_o^* E_1] \tag{83}$$

It is these cross-correlation terms on the right side of equation (83) that generate an image of the object.

3.2 Speckle Field

A speckle field is defined as a random intensity distribution of light over a plane. The generation of a speckle field can be created by taking a coherent wave and reflecting it off a "rough" surface. When the reflected wave front is observed using the same orientation of an incident wave front except with a rotation equal to the average angle of reflectance, an interference pattern emerges. The reason for this is because the rough surface adds a random amount of distance to the locally incident portion of the plane wave when compared to a non-rough surface. The random distance imparts a random phase to the locally incident wave. The wave front after reflection is a sum of all the locally incident portions of the plane wave via use of the Huygens-Fresnel wave principle. Since each locally incident wave portion has a random phase an

interference pattern emerges along the phase front of the reflected wave. This random phase is

best described as a random-walk phenomenon [48].
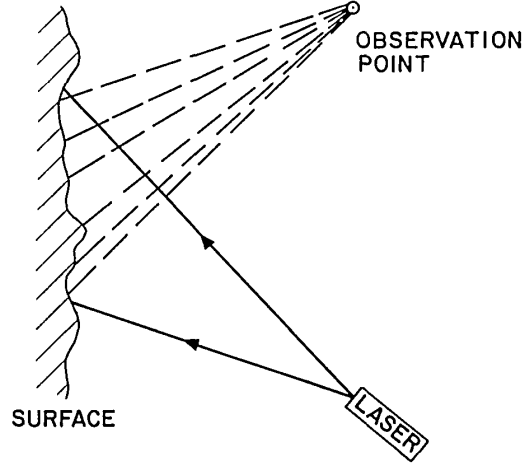
Figure 6: Free space geometry for speckle formation [48].

When viewing figure 5 the field at observation point is a superposition of all the different

paths that the field could have traveled from the laser to the surface and to the observation point.

Each path imparts a random phase to the field. The field at the observation point at a given point

in time is a summation of all the different paths.

$$\psi(x, y, z, t) = \sum_{m=1}^{\infty} A_m(x_m, y_m, z_m, t) e^{i(k(x_m, y_m, z_m) - \omega t + \phi_m)} \tag{84}$$

With the resulting intensity being:

$I_\psi(x, y, z, t)$

$$= \left\{ \sum_{m=1}^{\infty} A_m(x_m, y_m, z_m, t) e^{i(k(x_m, y_m, z_m) - \omega t + \phi_m)} \right\} \left\{ \sum_{m=1}^{\infty} A_m(x_m, y_m, z_m, t) e^{-i(k(x_m, y_m, z_m) -} \right. \tag{85}$$

The resulting cross terms give rise to the interference magnitude which determines if a

bright or dark spot is located at the observation point. Performing a sum over all the different

paths first and then performing the intensity calculation is akin to treating system as a random-walk phenomenon which is a well-studied classical problem [49-51]. Similar to a random-walk each scatterer on the reflecting surface can be represented by an amplitude ($|A_m|$) and phase (ϕ_m).

$$\psi_A(x, y, z, t) = \sum_{m=1}^{\infty} |A_m| e^{i\phi_m} \tag{86}$$

In doing this we will make two assumptions related to the scatterers. The first one is that each scattering element has its phase and amplitude statistically independent of each other. The second being that the phases have an equal probability to lie anywhere over the interval between ($-\pi \ and \ \pi$). With these two assumptions and following the mathematical proofs in [52] the results are the following. For many scatterers (m) the real and imaginary parts of the field for a given location are independent, zero mean, and identically distributed Gaussian random variables. The corresponding intensity has a probability density function of the form:

$$p(I) = \begin{cases} \dfrac{1}{\bar{I}} e^{-I/\bar{I}} & I \geq 0 \\ 0 & otherwise \end{cases} \tag{87}$$

where $\bar{I}$ is the intensity mean. This is a negative exponential distribution function that has a standard deviation equal to its mean. This leads to the contrast value of 1 for this generated speckle pattern as given by:

$$C = \sigma_I / \bar{I} \tag{88}$$

A random-walk phenomenon was used to describe the resulting field phase and amplitude located at an observation point in space. The resulting probability density function describing the intensity at that observation point is a negative exponential function with equal standard deviation and mean. The resulting contrast of 1 is a defining statistical characteristic of a speckle pattern.

3.2.1 Speckle Field Creation

A speckle field can be physically created with the use of a Phase-Only Spatial Light Modulator (SLM). A SLM is a pixelated plane which imparts a localized change in phase on the reflected field. When a field with a constant phase front is incident upon the SLM, the SLM imparts a random phase onto the local incident field akin to equation (86). By preforming a Fourier transform on the field post interaction with the SLM, a speckle field is created. This speckle field is deterministic even though a random phase was applied to each local phase front for two reasons. The first is due to the controllable nature of the imparted phase by the SLM. The second is that the Fourier plane phase front is calculable by Fourier transform. By controlling the local phase induced by the SLM on the SLM plane, one can produce any desired speckle field on the Fourier plane. This now leads to through specific control of the induced local phase on the SLM plane, the created speckle field on the Fourier plane can have a contrast equal to one (Rayleigh).

3.2.2 Rayleigh Speckles

The probability density function for a Rayleigh distribution is the following:

$$p_{Rayleigh}(x, \varsigma) = \frac{x}{\varsigma^2} e^{-x^2/2\varsigma^2} \tag{89}$$

where ς is a defining characteristic of the width of the Rayleigh distribution. The Rayleigh distribution has a corresponding expected value (mean) of:

$$E(x) = \varsigma \sqrt{\frac{\pi}{2}} \tag{90}$$

The variance is the expected value of a squared deviation of a random variable from its mean is given by:

$$Var(Z) = E[(Z - \mu)^2] \tag{91}$$

33

where Z is the random value and μ is the mean of the random value of Z. The variance for a Rayleigh distribution is the following:

$$Var = \frac{4 - \pi}{2} \varsigma^2 \tag{92}$$

With the standard deviation (σ) being the square root of the variance

$$\sigma = \sqrt{E[(Z - \mu)^2]} \tag{93}$$

The standard deviation for a Rayleigh distribution is:

$$\sigma = \sqrt{\frac{4 - \pi}{2} \varsigma^2} \tag{94}$$

Lastly with the root mean square (RMS) contrast defined as the standard deviation of the intensity over a defined region.

$$RMS\ Contrast = \sqrt{\frac{1}{M\,N} \sum_{i=0}^{N-1} \sum_{j=0}^{M-1} (I_{ij} - \bar{I})^2} \tag{95}$$

where I_{ij} is the ith, jth location in the field of view and $\bar{I}$ is the average intensity over the entire field of view. Now if we can use a Rayleigh distribution to describe the speckle intensity over a field of view:

$$p_{Rayleigh}(I, \varsigma) = \frac{I}{\varsigma^2} e^{-I^2/2\varsigma^2} \tag{96}$$

Then its standard deviation is exactly equal to the RMS contrast of that field. As described before the defining characteristic of a speckle field is when its contrast is equal to one. This means that for a Rayleigh distributed intensity field to have a contrast of 1, the defining characteristic of a Rayleigh distribution (ς) has the value of:

$$\varsigma = \sqrt{\frac{2}{4 - \pi}} \tag{97}$$

When the intensity distribution of a speckle field can be defined as a Rayleigh distribution with a

contras/σ equal to 1 we can define this speckle field as Rayleigh speckles.

Chapter 4

4. Group Delay via Frequency Ghost Imaging

In this chapter we will apply the concepts learned about the nature of light wave, in chapters 1 and 2, and ghost imaging, in chapter 3, to determine the group delay of an unknown optical pulse through analytical means. However, prior we must perform one more fundamental calculation that involves the correlation between a function and a random mask.

4.1   Fundamental cross correlation calculation

We begin with the fundamental theorem of calculus [53] which states that if the function $f(x)$ is continuous on the interval $[a, b]$ and it is the derivative of the function $F(x)$ then:

$$\int_a^b f(x)dx = F(a) - F(b) \tag{98}$$

The resulting value of this definite integral is easily calculated when there is a closed form solution to the integral of $f(x)$. When no closed form solution is available, one may use Reimann sum to approximate the solution, [53]. For $n < \infty$ and $n = \infty$, one such sum is expressed as follows.

$$\int_a^b f(x)dx = \lim_{n \to \infty} \sum_{i=0}^{n-1} f(x)\left(\frac{b-a}{n}\right) \tag{99}$$

The approximation above is called a left-hand side Reimann sum.   Other Reimann sum approximations include the right-hand side, or mid-point rule. The question becomes how would

one calculate second order correlation between function $f(x)$ and a random binary mask function $M(\xi)$? $M(\xi)$ *is* given as follows.

$$M(\xi) = \begin{Bmatrix} \mathbf{0} \\ \mathbf{1} \end{Bmatrix} \tag{100}$$

The second order correlation is given as follows.

$$G^{(2)}(x, \xi) = \langle \int_a^b f(x) dx \, M(\xi) \rangle \tag{101}$$

To start, we begin by applying a Reimann sum approximation to the integral to match up with the random binary mask function.

$$= \lim_{n \to \infty} \sum_{i=0}^{n-1} f(x) \left(\frac{b-a}{n} \right) \langle M(\chi)M(\xi) \rangle \tag{102}$$

Since the function $f(x)$ may not have zero mean and the mask function $M(\xi)$ will definitely not have a zero mean, the application of Isrellis theorem [54] needs to be applied to separate out the mean from the cross correlation.

$$= \lim_{n \to \infty} \sum_{i=0}^{n-1} f(x) \left(\frac{b-a}{n} \right) [\langle M(\chi)M(\xi) \rangle + \langle M(\chi) \rangle \langle M(\xi) \rangle] \tag{103}$$

$$= \lim_{n \to \infty} \sum_{i=0}^{n-1} f(x) \left(\frac{b-a}{n} \right) \langle M(\chi)M(\xi) \rangle + \langle \lim_{n \to \infty} \sum_{i=0}^{n-1} f(\chi) \left(\frac{b-a}{n} \right) \rangle \langle M(\xi) \rangle \tag{104}$$

Now that we have separated the mean (right term) from the cross-correlation (left term), we shall apply a Gaussian approximation to the mask function to the left term and compute the mean value associated with the mask function to the right term. A Gaussian approximation of the mask function allows the ability to vary the size of the mask function between values a and b.

$$= \lim_{n\to\infty} \sum_{i=0}^{n-1} f(\chi)\left(\frac{b-a}{n}\right) e^{\frac{-x^2+\xi^2}{4\Delta_m^2}} + \left\langle \lim_{n\to\infty} \sum_{i=0}^{n-1} f(\chi)\left(\frac{b-a}{n}\right)\right\rangle \frac{1}{2} \tag{105}$$

The term $e^{\frac{-x^2+\xi^2}{4\Delta_m^2}}$ is the Gaussian approximation of the mask function and when taking it to the extreme ($\Delta_m^2 \to \infty$), it becomes a delta function. If we also at the same time take both Reimann sums to their limits we get:

$$= \int_a^b f(\chi)\delta(\chi - \xi)d\chi + \left\langle \int_a^b f(\chi)d\chi \right\rangle \frac{1}{2} \tag{106}$$

And with completing the integrations

$$G^{(2)}(x,\xi) = f(\xi) + \left(\frac{F(b) - F(a)}{b-a}\right)\left(\frac{1}{2}\right) \tag{107}$$

The first term $f(\xi)$ is the cross-correlation term which is the derivative of the function $F(\xi)$ on the interval $[a, b]$. This term is the function $f(x)$ except with a change of variable. The second term is a combination of two terms: the mean value of an integral, and the average value associated with the random mask function. It might seem redundant to determine the original function $f(x)$ given that we used it to calculate a second order correlation between it and a random mask function resulting in it $f(\xi)$ plus a mean term but there is actually a scenario in which we know the resulting integral sum of a derivative function without knowing the derivative function itself.

4.2   Frequency ghost imaging in relation to spatial ghost imaging

As stated in chapter 3, a difference frequency monochromatic field of frequency (Ω) is generated as a result of an integral sum of the frequencies within the complex fields of $E_k(\omega)$ and $E_j^*(\omega)$. Where Ω is the frequency difference given that $\chi_{ijk}^{(2)}(\Omega; -\omega, \omega + \Omega)$.

$$P^{THz}(\Omega) = \int_{-\infty}^{\infty} \chi_{ijk}^{(2)}(\Omega; -\omega, \omega + \Omega)E_j^*(\omega)E_k(\omega + \Omega)d\omega \tag{108}$$

The initial phase of the difference frequency generated monochromatic field of frequency (Ω) is $\phi(\Omega)$ which is a definite integral sum of each phase difference between $E_k(\omega)$ and $E_j^*(\omega)$ that has a frequency difference of Ω, or equivalently the definite integral of the group delay of the polychromatic source.

$$\phi(\Omega) = \int_{-\infty}^{\infty} \phi(\omega + \Omega) - \phi(\omega)d\omega \tag{109}$$

We know from equation (4), in the introduction, that the negative frequency terms are conjugate values of the positive frequency values and we can represent complete amplitude and phase information through use of only the positive frequency terms, equation (25). When using correlated imaging in order to achieve tangible results, the negative frequency components will need to be separated from the positive frequency components which modifies equation (109) to.

$$\phi(\Omega) = \int_{0}^{\infty} \phi(\omega + \Omega) - \phi(\omega)d\omega \tag{110}$$

Here we have a definite integral consisting of only the positive frequency terms of a group delay. In the beginning of this chapter we saw that if we perform a second order correlation between a random binary mask function and a function that is the derivative $f(x)$ of a definite integral $F(b) - F(a)$ we can recover the derivative function $f(x)$. In comparison to $\phi(\omega + \Omega) - \phi(\omega) \equiv f(x)$ and $\phi(\Omega) \equiv F(b) - F(a)$. What is lacking is an equivalent mask function used in equation (101) for the second order correlation calculation. By creating a frequency to spatial conversion with a grating it will allow a binary spatial light modulator (BSLM) to control the frequencies of ω_k and ω_j that will contribute to the definite integral of $\phi(\Omega)$. The addition of a second binary

mask function will allow for the separation between the positive and negative frequencies allowing us to express equation (109) in (110). This leads to in the creation of fourth order correlation instead of a second order correlation. We can now take this fourth order correlation and relate it to spatial ghost imaging.

As you may recall there are two main equations when preforming spatial ghost imaging:

$$I_o^{(s)} = \iint O(x', y') I^{(s)}(x', y') dx' dy' \tag{111}$$

and

$$G(x, y) = \frac{1}{N} \sum_{s=1}^{N} I_o^{(s)} I^{(s)}(x, y) \tag{112}$$

When one equates frequency ghost imaging to spatial ghost imaging, the $\phi(\Omega)$ measurement is equivalent to the bucket detector $I_o^{(s)}$ measurement. The phase difference term between $E_k(\omega)$ and $E_j^*(\omega)$ is equivalent to the unknown spatial object $O(x', y')$; but instead of being spatially dependent (x', y'), it is frequency dependent $(\omega_k \ and \ \omega_j)$. The known variant quantity for spatial ghost imaging is $I^{(s)}(x, y)$. By creating a frequency to spatial conversion, the BSLM controls which frequencies contribute to the frequency-based bucket detector measurement $\phi(\Omega)$ and is equivalent to the known variant $I^{(s)}(x', y')$ and $I^{(s)}(x, y)$ in spatial ghost imaging. The two frequency ghost imaging equations equivalent to spatial ghost imaging are:

$$P^{THz}(\Omega) = \iiint_{-\infty}^{\infty} \chi_{ijk}^{(2)}(\Omega; \omega, \omega + \Omega) M(\xi) E_j^*(\omega) M(\xi') E_k(\omega + \Omega) d\omega d\xi d\xi' \tag{113}$$

and

$$G(\xi, \xi', \Omega) = \frac{1}{N} \sum_{s=1}^{N} P^{THz}(\Omega) M(\xi) M(\xi') \tag{114}$$

4.3   Experimental configuration for frequency ghost imaging

The following is a proposed schematic of an experimental setup for the implementation of frequency ghost imaging.
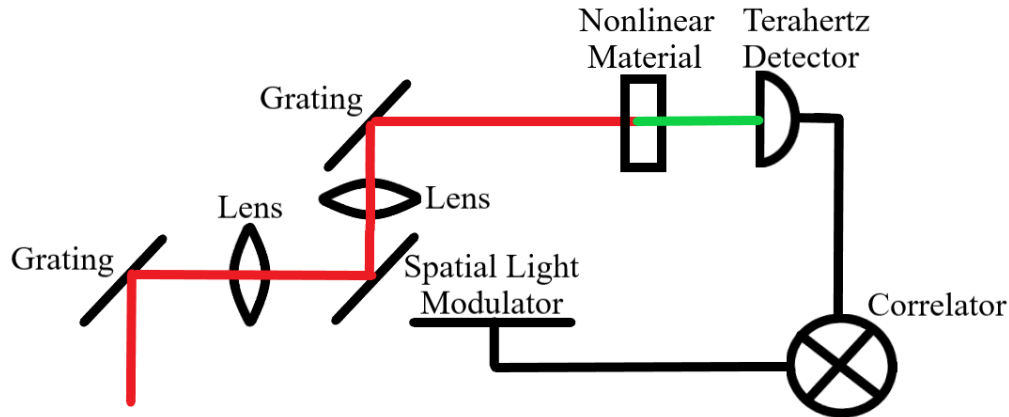
Figure 7: An unknown ultrafast optical pulse is first incident upon a grating lens pair. This pair is used to perform a frequency to spatial conversion. The separated frequencies are then incident upon a binary spatial light modulator (BSLM) that randomly selects frequencies to remove. The optical pulse is then reconstructed by a second grating lens pair without the removed optical frequencies. This new pulse then passes through a nonlinear material which performs a frequency mixing on the optical pulse via difference frequency generation. For unknown optical pulses with a central wavelength in the 810nm range this produces a terahertz (THz) pulse. A correlator then corelates the measured phase for a given THz frequency measured by a THz detector with the orientation of the BSLM through many different BSLM realizations.

A femtosecond pulse with unknown phase characteristics is first incident upon a grating lens pair which spatially spreads the different frequency components. A BSLM then randomly selects which frequency components within the unknown pulse to be incident upon a nonlinear material. A second grating lens pair is used to reconstruct the pulse without the disregarded frequencies chosen by the BSLM. The resulting pulse is now incident upon a nonlinear material which preforms frequency mixing. Through difference frequency generation a terahertz pulse is generated which is then measured by a terahertz detector. Taking a closer look at the BSLM as a

first order approximation the frequencies across the BSLM can be described in a linear approximation.

0	0	0	0	0	0
1	1	1	1	1	1

$$\cdots \quad \omega_{-2} \quad \omega_{-1} \quad \omega_0 \quad \omega_{+1} \quad \omega_{+2} \quad \omega_{+3} \quad \cdots$$

Figure 8: A first order linear approximation of the optical angular frequencies that the binary spatial light modulator can pass or not pass.

When ω_i and ω_{i+1} are both passed through the BSLM, the nonlinear material produces the positive frequency

$$\Delta\omega = \omega_{i+1} - \omega_i \tag{115}$$

through difference frequency generation. As seen in chapter 2, monochromatic frequency creation through difference frequency generation, the initial phase of the generated frequency is equal to the phase difference between the two frequencies. Also seen in chapter 2, polychromatic frequency creation through difference frequency generation, the initial phase of a specific generated frequency is an integral sum of the initial phase difference between all the monochromatic frequencies that could generate the specific frequency. With our control over the BSLM we can construct a linear approximation of the phase differences that contribute to the integral sum for a specific generated frequency's initial phase. Using equation (102) as an example for a specific generated frequency of $\Delta\omega$, we know the contributing frequencies and their contributing phase differences. This is visualized in figure 8.

0	0	0	0
1	1	1	1

$$\ldots \quad \omega_{-2} - \omega_{-1} \qquad \omega_{-1} - \omega_{0} \qquad \omega_{0} - \omega_{1} \qquad \omega_{1} - \omega_{2} \quad \ldots$$

Figure 9: A first order linear approximation of the difference frequency generation between two optical angular frequencies that contribute to the phase of a newly generated frequency.

The nonlinear material will generate this frequency $\Delta\omega$ for all consecutive ω_i and ω_{i+1}, resulting in initial phase of frequency $\Delta\omega$ that is a sum of all consecutive ω_i and ω_{i+1} due to BSLM. To expand this specific monochromatic field generation of frequency $\Delta\omega$ to a polychromatic field generation, we perform a matrix multiplication of figure 7.

	$\ldots$	$0\vert1$ ω_{-2}	$0\vert1$ ω_{-1}	$0\vert1$ ω_{0}	$0\vert1$ ω_{1}	$0\vert1$ ω_{2}	$\ldots$
$\vdots$							
$0\vert1$ ω_{-2}			$(0\vert1)(0\vert1)(\omega_{-1}-\omega_{-2})$	$(0\vert1)(0\vert1)(\omega_{0}-\omega_{-2})$	$(0\vert1)(0\vert1)(\omega_{1}-\omega_{-2})$		
$0\vert1$ ω_{-1}			$(0\vert1)(0\vert1)(\omega_{-1}-\omega_{-1})$	$(0\vert1)(0\vert1)(\omega_{0}-\omega_{-1})$	$(0\vert1)(0\vert1)(\omega_{1}-\omega_{-1})$		
$0\vert1$ ω_{0}			$(0\vert1)(0\vert1)(\omega_{-1}-\omega_{0})$	$(0\vert1)(0\vert1)(\omega_{0}-\omega_{0})$	$(0\vert1)(0\vert1)(\omega_{1}-\omega_{0})$		
$0\vert1$ ω_{1}			$(0\vert1)(0\vert1)(\omega_{-1}-\omega_{1})$	$(0\vert1)(0\vert1)(\omega_{0}-\omega_{1})$	$(0\vert1)(0\vert1)(\omega_{1}-\omega_{1})$		
$0\vert1$ ω_{2}			$(0\vert1)(0\vert1)(\omega_{-1}-\omega_{2})$	$(0\vert1)(0\vert1)(\omega_{0}-\omega_{2})$	$(0\vert1)(0\vert1)(\omega_{1}-\omega_{2})$		
$\vdots$							

Table 1: Optical angular frequencies located along the top and side of the table are controlled by the binary spatial light modulator (BSLM). A given generated frequency created through difference frequency generation (DFG) can be found within the table along a diagonal. For a given BSLM realization only certain optical angular frequencies can contribute to DFG.

Along the top and side of this matrix we have the frequencies passed by the BSLM. Along each diagonal of this matrix, we have a newly generated monochromatic field. A given diagonal is a specific example given by equation (115) and seen in figure 8. By taking the frequencies along

the top to be positive and the frequencies along the side to be negative, the central diagonal of this matrix represents the newly generated frequency of 0 rads/s. Diagonals above the central diagonal are newly generated positive frequencies and increase in magnitude the further away from the diagonal. Diagonals below the central diagonal are newly generated negative frequencies that increase in negative magnitude the further away from the diagonal.

The bucket detector measurement, equation (113), is a phase measurement with frequency $\Delta\omega$ which corresponds to a given diagonal within the matrix. A fourth order correlation between the two mask functions and the corresponding source frequencies gives measure of group delay (GD) of the incident pulse. As the bucket detector measurement $\Delta\omega$ decreases in frequency, the better the approximation of group delay will be. There is a caveat though to achieving a better estimation of group delay; a greater number of realizations need to be taken due to the increased segmentation of group delay.

4.4 Analytical calculation of group delay via frequency ghost imaging

To determine the group delay for an unknown optical pulse using frequency ghost imaging we must complete a fourth order correlation calculation akin to the second order calculation preformed at the beginning of chapter with an accurate accounting of all possible changes in phase.

4.4.1 Field, Phase, Mask, and Measurements in frequency ghost imaging

First, we assume that the input field is separable in x and t (x is perpendicular to the direction of travel).

$$E_{in}(x,t) = a_{in}(x)a_{in}(t) \tag{116}$$

In the frequency domain we have

$$E_{in}(\omega,t) = a_{in}(x)a_{in}(\omega) \tag{117}$$

Where we have made use of the Fourier transform.

$$a_{in}(\omega) = \int_{-\infty}^{\infty} a_{in}(t)e^{i\omega t}\, dt \tag{118}$$

We have $\omega = \varpi - \omega_0$ with ω_0 being the central angular frequency.

The unknown optical pulse is first incident upon a grating which will spatially decomposed into different frequency components that make up the unknown optical pulse. In accordance with Martinez [55], a frequency dependent phase is induced upon the field when the field interacts with the grating G1.

$$E_1(x_1, \omega) = E_{in}(\alpha x_1, \omega)e^{ik\beta \omega x_1} \tag{119}$$

In a short aside we will follow Martinez's work [55] so see the derivation of the frequency dependent phase is induced from the interaction of the optical pulse with a grating.

Aside

With an input field given by $a(x, \omega)$ the spatial Fourier transform $A(\xi, \omega)$ is:

$$A(\xi, \omega) = \int_{-\infty}^{\infty} a(x, \omega)e^{i2\pi\xi x}dx \tag{120}$$

The input field as a superposition of plane waves traveling at different angles. $A(\xi, \omega)$ is a Dirac function $\delta(\xi - \xi_0)$ when:

$$a(x, \omega) = e^{i2\pi\xi_0 x} \tag{121}$$

A plane wave propagating at angle $\Delta\gamma$ has a phase of $(2\pi/\lambda)[\sin(\Delta\gamma)x + \cos(\Delta\gamma)z]$. If $\Delta\gamma \cong \sin(\Delta\gamma) = \xi_0\lambda$ and we have constant z then the amplitude is given above using the small angle approximation.

An incident field is to be deflected by an angle $\alpha \Delta \gamma$. The increase in angle by a factor of α is matched to an equivalent increase in the spatial frequency. The resulting amplitude at spatial frequency ξ would then be proportional to the incident amplitude at frequency ξ / α thus:

$$A_T(\xi, \omega) = A\left(\frac{\xi}{\alpha}, \omega\right) \tag{122}$$

The transmitted field A_T is found by taking the inverse Fourier transform of the above equation. The dispersion due to the grating $(\beta \omega)$ is added by multiplying a frequency-dependent phase factor that defines a rotation

$$a_T(x_2, \omega) = e^{ik\beta\omega x_2} F^{-1}\left[A_T\left(\frac{\xi}{\alpha}\right)\right] = e^{ik\beta\omega x_2} a(x_2 \alpha) \tag{123}$$

In determining the values of α and β, they are determined to be:

$$\alpha = \frac{\cos(\theta_0)}{\cos(\gamma_0)} \tag{124}$$

$$\beta = \frac{2\pi c m}{\omega_0^2 d \cos(\gamma_0)} \tag{125}$$

where γ_0 and θ_0 are the incident and transmitted angles respectively, m is the grating order, and d is the grating spacing.

End Aside

After the first grating the field then undergoes a Fourier transform performed by lens L₁. The field incident upon the filter is:

$$E_2(\chi, \omega) = a_{in}(\omega) \int_{-\infty}^{\infty} a_{in}(\alpha x_1) e^{i\left(k\beta\omega - \frac{k\chi}{f}\right)x_1} dx_1 \tag{126}$$

where f is the focal length of the Fourier transform lens. The field just after the filter is:

$$E_3(\chi, \omega) = a_{in}(\omega) M_n(\chi) \int_{-\infty}^{\infty} a_{in}(\alpha x_1) e^{ik\left(\beta\omega - \frac{\chi}{f}\right)x_1} dx_1 \tag{127}$$

Now if we suppose that the input spatial profile is of a Gaussian distribution

$$a_{in}(x) = a_0 e^{-\frac{x^2}{D^2}} \tag{128}$$

where D is the beam size on the grating, we can integrate with respect to x_1 and arrive at

$$E_3'(\chi, \omega) = \frac{\sqrt{\pi} D a_0}{\alpha} a_{in}(\omega) M_n(\chi) e^{-\frac{k^2 D^2}{4f^2 \alpha^2}(\chi - f\beta\omega)^2} \tag{129}$$

We perform a second Fourier transform by a second lens L₂ from $M(\chi)$ plane to the second grating:

$$E_4(x_2, \omega) = \frac{\sqrt{\pi} D a_0}{\alpha} a_{in}(\omega) \int_{-\infty}^{\infty} M_n(\chi) e^{-\frac{k^2 D^2}{4f^2 \alpha^2}(\chi - f\beta\omega)^2} e^{-i\frac{kx_2}{f}\chi} d\chi \tag{130}$$

Considering the previous equation with the following $E_1(x_1, \omega) = E_{in}(\alpha x_1, \omega) e^{ik\beta\omega x_1}$ in finding

the effect of the second grating but with a reverse effect, i.e., $E_5(x_3, \omega) = E_4\left(\frac{x_3}{\alpha}, \omega\right) e^{-i\frac{k\beta\omega}{\alpha} x_3}$ we

arrive at:

$$E_5(x_3, \omega) = \frac{\sqrt{\pi} D a_0}{\alpha} a_{in}(\omega) \int_{-\infty}^{\infty} M_n(\chi) e^{-\frac{k^2 D^2}{4f^2 \alpha^2}(\chi - f\beta\omega)^2} e^{-i\frac{kx_3}{\alpha f}\chi} e^{-i\frac{k\beta\omega}{\alpha} x_3} d\chi \tag{131}$$

The output field in general is given by

$$E_{out}(x_3, \omega) = \int_{-\infty}^{\infty} d\chi \int_{-\infty}^{\infty} a_{in}(\alpha x_1, \omega) M(\chi) e^{-i\frac{k\beta\omega}{\alpha} x_3} e^{-i\frac{kx_3}{\alpha f}\chi} e^{-i\frac{k\chi}{f} x_1} e^{ik\beta\omega x_1} dx_1 \tag{132}$$

If we consider the Gaussian profile in x:

$$a_{in}(\alpha x_1, \omega) = a_{in}(\omega) a_{in}(\alpha x_1) = a_{in}(\omega) e^{-\frac{\alpha^2 x_1^2}{D^2}} \tag{133}$$

$$E_{out}(x_3, \omega) = \int_{-\infty}^{\infty} d\chi \int_{-\infty}^{\infty} a_{in}(\omega) M(\chi) e^{-\frac{\alpha^2 x_1^2}{D^2}} e^{-i\frac{k\beta\omega}{\alpha} x_3} e^{-i\frac{kx_3}{\alpha f}\chi} e^{-i\frac{k\chi}{f} x_1} e^{ik\beta\omega x_1} dx_1 \tag{134}$$

$$= \int_{-\infty}^{\infty} a_{in}(\omega) e^{-i\frac{k\beta\omega}{\alpha} x_3} e^{-\frac{k^2 D^2(f\beta\omega - \chi)^2}{4f^2 \alpha^2}} e^{-i\frac{kx_3}{\alpha f}\chi} M(\chi) d\chi \tag{135}$$

The resulting field is achieved without the using a frequency filter but with light interaction with two lenses and two gratings. Now the field generated by the second order nonlinear process of difference frequency generation is:

$$P^{THz}(\Omega) = \int_{-\infty}^{\infty} \chi_{ijk}^{(2)}(\Omega; \omega, \omega + \Omega) E_j^*(\omega) E_k(\omega + \Omega) d\omega \qquad (136)$$

Considering the field generated by the second order nonlinear process in equation (136), the frequency filter shall be approximated as:

$$\langle M(\chi) M(\chi') \rangle = e^{-\frac{\chi^2 + \chi'^2}{4\Delta_M^2}} e^{-\frac{(\chi - \chi')^2}{2\sigma_M^2}} \qquad (137)$$

And applying this process to the modulated field above (135):

$$P^{THz}(x_3, \Omega) = \int_{-\infty}^{\infty} d\omega \chi_{ijk}^{(2)}(\Omega; \omega, \omega' = \omega + \Omega) \int_{-\infty}^{\infty} a_{in}(\omega) e^{-i\frac{k\beta\omega}{\alpha}x_3} e^{-\frac{k^2 D^2 (f\beta\omega - \chi)^2}{4f^2\alpha^2}} e^{-i\frac{kx_3}{\alpha f}\chi} d\chi$$

$$\int_{-\infty}^{\infty} a_{in}^*(\omega') e^{i\frac{k\beta\omega'}{\alpha}x_3} e^{-\frac{k^2 D^2 (f\beta\omega' - \chi')^2}{4f^2\alpha^2}} e^{i\frac{kx_3}{\alpha f}\chi'} e^{-\frac{\chi^2 + \chi'^2}{4\Delta_M^2}} e^{-\frac{(\chi - \chi')^2}{2\sigma_M^2}} d\chi' \qquad (138)$$

Being frequency ghost imaging, the bucket detector is a complex value. Next chapter will elaborate further on the achieved results. For now, the response function of the detector is taken as $h(\Omega')$

$$\int_{-\infty}^{\infty} h(\Omega' - \Omega) d\Omega \qquad (139)$$

4.4.2   Fourth order analytical calculation of group delay via frequency ghost imaging

With this the fourth order correlation function for frequency ghost imaging is:

$$G^2(x_3, \xi, \xi', \Omega') = \langle \int_{-\infty}^{\infty} d\Omega \, h(\Omega' - \Omega) \, P^{THz}(x_3, \Omega) M(\xi), M(\xi') \rangle \qquad (140)$$

$$= \int_{-\infty}^{\infty} d\Omega \, h(\Omega' - \Omega) \int_{-\infty}^{\infty} d\omega \chi_{ijk}^{(2)}(\Omega; \omega, \omega' = \omega + \Omega) \int_{-\infty}^{\infty} a_{in}(\omega) e^{-i\frac{k\beta\omega}{\alpha}x_3} e^{-\frac{k^2 D^2 (f\beta\omega - \chi)^2}{4f^2\alpha^2}} e^{-i\frac{kx_3}{\alpha f}\chi} d\chi \qquad (141)$$

$$\times \int_{-\infty}^{\infty} a_{in}^*(\omega') e^{i\frac{k\beta\omega'}{\alpha}x_3} e^{-\frac{k^2 D^2 (f\beta\omega' - \chi')^2}{4f^2\alpha^2}} e^{i\frac{kx_3}{\alpha f}\chi'} d\chi' \langle M(\chi)M(\chi')M(\xi)M(\xi') \rangle$$

In reviewing the on-axis results ($x_3 = 0$) for the fourth order correlation function, we end up with

is a matrix of size $\xi \times \xi'$ with complex values associated with the generated frequency Ω'. The

mask functions of $M(\xi)$ and $M(\xi')$ are represented in figure 7 with their matrix multiplied elements

$M(\xi) \times M(\xi')$ seen in table 1. Figure 8 represents a given diagonal within the $M(\xi) \times M(\xi')$

matrix. Applying the Gaussian moment theorem to equation (141), we get:

$$G^2(x_3, \xi, \xi', \Omega') =$$

$$\int_{-\infty}^{\infty} d\Omega\, h(\Omega' - \Omega) \int_{-\infty}^{\infty} d\omega \chi_{ijk}^{(2)}(\Omega; \omega, \omega' = \omega + \Omega) \int_{-\infty}^{\infty} a_{in}(\omega) e^{-i\frac{k\beta\omega}{\alpha}x_3} e^{-\frac{k^2 D^2 (f\beta\omega - \chi)^2}{4f^2\alpha^2}} e^{-i\frac{kx_3}{\alpha f}\chi} d\chi$$

$$(142)$$

$$\times \int_{-\infty}^{\infty} a_{in}^*(\omega') e^{i\frac{k\beta\omega'}{\alpha}x_3} e^{-\frac{k^2 D^2 (f\beta\omega' - \chi')^2}{4f^2\alpha^2}} e^{i\frac{kx_3}{\alpha f}\chi'} d\chi' [\langle M(\chi)M(\chi') \rangle \langle M(\xi)M(\xi') \rangle$$

$$+ \langle M(\chi)M(\xi) \rangle \langle M(\chi')M(\xi') \rangle + \langle M(\chi)M(\xi') \rangle \langle M(\chi')M(\xi) \rangle]$$

This previous line gives the following three terms: A DC Intensity term, and two mirrored terms.

One mirrored term has positive frequencies on the left side of the diagonal and negative

frequencies on the right side of the diagonal. The other mirrored term has negative frequencies on

the left side of the diagonal and positive frequencies on the right side of the diagonal

The DC term (which corresponds to the matrix diagonal) is expressed by:

$$\int_{-\infty}^{\infty} d\Omega\, h(\Omega' - \Omega) \int_{-\infty}^{\infty} d\omega \chi_{ijk}^{(2)}(\Omega; \omega, \omega' = \omega + \Omega) |E_{out}(x_3, \omega)|^2 \langle M(\xi)M(\xi') \rangle \qquad (143)$$

One mirrored term is expressed by:

$$\int_{-\infty}^{\infty} d\Omega\, h(\Omega' - \Omega) \int_{-\infty}^{\infty} d\omega \chi_{ijk}^{(2)}(\Omega; \omega, \omega' = \omega + \Omega)$$

$$(144)$$

$$\times \int_{-\infty}^{\infty} a_{in}(\omega) e^{-i\frac{k\beta\omega}{\alpha}x_3} e^{-\frac{k^2 D^2 (f\beta\omega - \chi)^2}{4f^2\alpha^2}} e^{-i\frac{kx_3}{\alpha f}\chi} d\chi \langle M(\chi)M(\xi) \rangle$$

$$\times \int_{-\infty}^{\infty} a_{in}^*(\omega')e^{i\frac{k\beta\omega'}{\alpha}x_3}e^{-\frac{k^2D^2(f\beta\omega'-\chi')^2}{4f^2\alpha^2}}e^{i\frac{kx_3}{\alpha f}\chi'}d\chi'\,\langle M(\chi')M(\xi')\rangle$$

The other mirrored term is expressed by:

$$\int_{-\infty}^{\infty} d\Omega\, h(\Omega'-\Omega)\int_{-\infty}^{\infty} d\omega \chi_{ijk}^{(2)}(\Omega;\omega,\omega'=\omega+\Omega)$$

$$\times \int_{-\infty}^{\infty} a_{in}(\omega)e^{-i\frac{k\beta\omega}{\alpha}x_3}e^{-\frac{k^2D^2(f\beta\omega-\chi)^2}{4f^2\alpha^2}}e^{-i\frac{kx_3}{\alpha f}\chi}d\chi\,\langle M(\chi)M(\xi')\rangle \tag{145}$$

$$\times \int_{-\infty}^{\infty} a_{in}^*(\omega')e^{i\frac{k\beta\omega'}{\alpha}x_3}e^{-\frac{k^2D^2(f\beta\omega'-\chi')^2}{4f^2\alpha^2}}e^{i\frac{kx_3}{\alpha f}\chi'}d\chi'\,\langle M(\chi')M(\xi)\rangle$$

Negative frequency is related the mask selection on ω and ω'. When ω' is smaller than ω the resulting generated frequency Ω is negative. We begin with equation (116) as a complex representation of an unknown polychromatic field. Through equation (136), we generate a new polychromatic field by difference frequency generation. The resulting Fourier transform of the measured polarization signal in the temporal domain $P^{THz}(x_3, t)$ generated through difference frequency generation gives both positive and negative frequencies. This is true of all propagating electric fields; a simple example of this is the Fourier transform of a monochromatic wave as seen in the introduction chapter:

$$F[\cos(2\pi f_0 t + \theta)] = \frac{1}{2}e^{i\theta}\delta(f-f_0) + \frac{1}{2}e^{-i\theta}\delta(f+f_0) \tag{146}$$

The complete solution of equations (143) through (145) which are equivalent to the right-hand side of the previous equation (146) involves both positive and negative frequencies which would yield no results if not for control over the bucket detector. By using only, the positive frequency complex values measured by the bucket detector one can achieve tangible results. Knowing that

the two mirrored terms are but complex conjugates of each other; hence in calculating for one; the other can be easily determined. Beginning with one of the mirrored terms:

$$G^2(x_3,\xi,\xi',\Omega') = \int_{-\infty}^{\infty} d\Omega\, h(\Omega'-\Omega) \int_{-\infty}^{\infty} d\omega \chi_{ijk}^{(2)}(\Omega;\omega,\omega'=\omega+\Omega)\,|E_{out}(x_3,\omega)|^2 \langle M(\xi)M(\xi')\rangle$$

$$+ \int_{-\infty}^{\infty} d\Omega\, h(\Omega'-\Omega) \int_{-\infty}^{\infty} d\omega \chi_{ijk}^{(2)}(\Omega;\omega,\omega'=\omega+\Omega)$$

$$\times \int_{-\infty}^{\infty} a_{in}(\omega) e^{-i\frac{k\beta\omega}{\alpha}x_3} e^{-\frac{k^2 D^2 (f\beta\omega-\chi)^2}{4f^2\alpha^2}} e^{-i\frac{kx_3}{\alpha f}\chi} d\chi \,\langle M(\chi)M(\xi)\rangle$$

$$\times \int_{-\infty}^{\infty} a_{in}^*(\omega') e^{i\frac{k\beta\omega'}{\alpha}x_3} e^{-\frac{k^2 D^2 (f\beta\omega'-\chi')^2}{4f^2\alpha^2}} e^{i\frac{kx_3}{\alpha f}\chi'} d\chi' \,\langle M(\chi')M(\xi')\rangle$$

(147)

In order to simplify the integration involving the $\chi_{ijk}^{(2)}$ term, I want to describe $a_{in}(\omega)$ and $a_{in}^*(\omega')$ in terms of the temporal domain. By doing so the integration involving $\int_{-\infty}^{\infty} d\omega \chi_{ijk}^{(2)}(\Omega;\omega,\omega' = \omega + \Omega)$ can be dropped because the $\chi_{ijk}^{(2)}$ term is a multiplication in the temporal domain and not a convolution. Then after the temporal multiplication has been completed, we can Fourier transform back to the frequency domain.

$$= \int_{-\infty}^{\infty} d\Omega\, h(\Omega'-\Omega) \int_{-\infty}^{\infty} dt\, e^{i\Omega t} \chi_{ijk}^{(2)}(t;t',t')|E_{out}(x_3,t')|^2 \langle M(\xi)M(\xi')\rangle$$

$$+ \int_{-\infty}^{\infty} d\Omega\, h(\Omega'-\Omega) \int_{-\infty}^{\infty} dt'\, e^{i\Omega t'} \chi_{ijk}^{(2)}(t';\omega,\omega')$$

$$\times \int_{-\infty}^{\infty} d\omega\, e^{-i\frac{k\beta\omega}{\alpha}x_3} e^{-i\omega t'} a_{in}(\omega) \int_{-\infty}^{\infty} e^{-\frac{k^2 D^2 (f\beta\omega-\chi)^2}{4f^2\alpha^2}} e^{-i\frac{kx_3}{\alpha f}\chi} d\chi \,\langle M(\chi)M(\xi)\rangle$$

$$\times \int_{-\infty}^{\infty} d\omega'\, e^{i\frac{k\beta\omega'}{\alpha}x_3} e^{i\omega't'} a_{in}^*(\omega') \int_{-\infty}^{\infty} e^{-\frac{k^2 D^2 (f\beta\omega'-\chi')^2}{4f^2\alpha^2}} e^{i\frac{kx_3}{\alpha f}\chi'} d\chi' \,\langle M(\chi')M(\xi')\rangle$$

(148)

Next, we insert the mathematical description of the mask function:

$$= \int_{-\infty}^{\infty} d\Omega\, h(\Omega'-\Omega) \int_{-\infty}^{\infty} dt\, e^{i\Omega t} \chi_{ijk}^{(2)}(t;t',t')|E_{out}(x_3,t')|^2 \langle M(\xi)M(\xi')\rangle$$

(149)

$$+ \int_{-\infty}^{\infty} d\Omega \, h(\Omega' - \Omega) \int_{-\infty}^{\infty} dt' \, e^{i\Omega t'} \chi_{ijk}^{(2)}(t'; \omega, \omega')$$

$$\times \int_{-\infty}^{\infty} d\omega \, e^{-i\frac{k\beta\omega}{\alpha}x_3} e^{-i\omega t'} a_{in}(\omega) \int_{-\infty}^{\infty} e^{-\frac{k^2 D^2 (f\beta\omega - \chi)^2}{4f^2\alpha^2}} e^{-i\frac{kx_3}{\alpha f}\chi} e^{-\frac{\chi^2+\xi^2}{4\Delta_M^2}} e^{-\frac{(\chi-\xi)^2}{2\sigma_M^2}} d\chi$$

$$\times \int_{-\infty}^{\infty} d\omega' e^{i\frac{k\beta\omega'}{\alpha}x_3} e^{i\omega' t'} a_{in}^*(\omega') \int_{-\infty}^{\infty} e^{-\frac{k^2 D^2 (f\beta\omega' - \chi')^2}{4f^2\alpha^2}} e^{i\frac{kx_3}{\alpha f}\chi'} e^{-\frac{\chi'^2+\xi'^2}{4\Delta_M^2}} e^{-\frac{(\chi'-\xi')^2}{2\sigma_M^2}} d\chi'$$

We integrate with respect to χ and χ':

$$= \int_{-\infty}^{\infty} d\Omega \, h(\Omega' - \Omega) \int_{-\infty}^{\infty} dt \, e^{i\Omega t} \chi_{ijk}^{(2)}(t; t', t') |E_{out}(x_3, t')|^2 \langle M(\xi) M(\xi') \rangle$$

$$+ \int_{-\infty}^{\infty} d\Omega \, h(\Omega' - \Omega) \int_{-\infty}^{\infty} dt' \, e^{i\Omega t'} \chi_{ijk}^{(2)}(t'; \omega, \omega') e^{-\frac{\xi^2+\xi'^2}{4\Delta_M^2}} \tag{150}$$

$$\times \int_{-\infty}^{\infty} d\omega \, e^{-i\frac{k\beta\omega}{\alpha}x_3} e^{-i\omega t'} a_{in}(\omega) e^{-\frac{\left(\frac{kx_3}{\alpha f}\right)^2 + 4i\left(\frac{kx_3}{\alpha f}\right)\left[\frac{k^2 D^2}{4f^2\alpha^2}f\beta\omega + \frac{1}{2\sigma_M^2}\xi\right] + 4\frac{k^2 D^2}{4f^2\alpha^2}\left[\frac{1}{4\Delta_M^2}(f\beta\omega)^2 + \frac{1}{2\sigma_M^2}(f\beta\omega - \xi)^2\right] + \frac{1}{4\Delta_M^2}\frac{1}{2\sigma_M^2}\xi^2}{4\left(\frac{k^2 D^2}{4f^2\alpha^2} + \frac{1}{4\Delta_M^2} + \frac{1}{2\sigma_M^2}\right)}}$$

$$\times \int_{-\infty}^{\infty} d\omega' \, e^{-i\frac{k\beta\omega'}{\alpha}x_3} e^{-i\omega' t'} a_{in}^*(\omega') e^{-\frac{\left(\frac{kx_3}{\alpha f}\right)^2 - 4i\left(\frac{kx_3}{\alpha f}\right)\left[\frac{k^2 D^2}{4f^2\alpha^2}f\beta\omega' + \frac{1}{2\sigma_M^2}\xi'\right] + 4\frac{k^2 D^2}{4f^2\alpha^2}\left[\frac{1}{4\Delta_M^2}(f\beta\omega')^2 + \frac{1}{2\sigma_M^2}(f\beta\omega' - \xi')^2\right] + \frac{1}{4\Delta_M^2}\frac{1}{2\sigma_M^2}\xi'^2}{4\left(\frac{k^2 D^2}{4f^2\alpha^2} + \frac{1}{4\Delta_M^2} + \frac{1}{2\sigma_M^2}\right)}}$$

A rearrangement of the σ_M^2 terms result in:

$$= \int_{-\infty}^{\infty} d\Omega \, h(\Omega' - \Omega) \int_{-\infty}^{\infty} dt \, e^{i\Omega t} \chi_{ijk}^{(2)}(t; t', t') |E_{out}(x_3, t')|^2 \langle M(\xi) M(\xi') \rangle$$

$$+ \int_{-\infty}^{\infty} d\Omega \, h(\Omega' - \Omega) \int_{-\infty}^{\infty} dt' \, e^{i\Omega t'} \chi_{ijk}^{(2)}(t'; \omega, \omega') e^{-\frac{\xi^2+\xi'^2}{4\Delta_M^2}} \tag{151}$$

$$\times \int_{-\infty}^{\infty} d\omega \, e^{-i\frac{k\beta\omega}{\alpha}x_3} e^{-i\omega t'} a_{in}(\omega) e^{-\frac{(k\sigma_M)^2 x_3^2 + i\left(\frac{kx_3}{\alpha f}\right)\left[\frac{k^2 D^2 \sigma_M^2}{f^2\alpha^2}f\beta\omega + 2\xi\right] + \frac{k^2 D^2}{2f^2\alpha^2}\left[\frac{\sigma_M^2}{2\Delta_M^2}(f\beta\omega)^2 + (f\beta\omega - \xi)^2\right] + \frac{1}{2\Delta_M^2}\xi^2}{\left(\frac{k^2 D^2 \sigma_M^2}{f^2\alpha^2} + \frac{\sigma_M^2}{\Delta_M^2} + 2\right)}}$$

$$\times \int_{-\infty}^{\infty} d\omega' \, e^{-i\frac{k\beta\omega'}{\alpha}x_3} e^{-i\omega' t'} a_{in}^*(\omega') e^{-\frac{(k\sigma_M)^2 x_3^2 + i\left(\frac{kx_3}{\alpha f}\right)\left[\frac{k^2 D^2 \sigma_M^2}{f^2\alpha^2}f\beta\omega' + 2\xi'\right] + \frac{k^2 D^2}{2f^2\alpha^2}\left[\frac{\sigma_M^2}{2\Delta_M^2}(f\beta\omega')^2 + (f\beta\omega' - \xi')^2\right] + \frac{1}{2\Delta_M^2}\xi'^2}{\left(\frac{k^2 D^2 \sigma_M^2}{f^2\alpha^2} + \frac{\sigma_M^2}{\Delta_M^2} + 2\right)}}$$

Taking $\Delta_M \to \infty$

$$\rightarrow \int_{-\infty}^{\infty} d\Omega\, h(\Omega' - \Omega) \int_{-\infty}^{\infty} dt\, e^{i\Omega t}\, \chi_{ijk}^{(2)}(t; t', t')\, |E_{out}(x_3, t')|^2\, e^{-\frac{(\xi - \xi')^2}{2\sigma_M^2}}$$

$$+ \int_{-\infty}^{\infty} d\Omega\, h(\Omega' - \Omega) \int_{-\infty}^{\infty} dt'\, e^{i\Omega t'}\, \chi_{ijk}^{(2)}(t'; \omega, \omega')\, e^{-\frac{2\left(\frac{k\sigma_M}{\alpha f}\right)^2 x_3^2 + i\left(\frac{2k}{\alpha f}\right)x_3(\xi - \xi')}{\left(\frac{k^2 D^2 \sigma_M^2}{f^2 \alpha^2} + 2\right)}}$$

$$\times \int_{-\infty}^{\infty} d\omega\, e^{-i\omega t'}\, a_{in}(\omega)\, e^{-\frac{k\beta}{\alpha}\left[1+\left(1+\frac{2f^2\alpha^2}{k^2 D^2 \sigma_M^2}\right)^{-1}\right]x_3 \omega}\, e^{-\frac{1}{2\sigma_M^2\left(1+\frac{2f^2\alpha^2}{k^2 D^2 \sigma_M^2}\right)}(f\beta\omega - \xi)^2}$$

$$\times \int_{-\infty}^{\infty} d\omega'\, e^{-i\omega' t'}\, a_{in}^*(\omega')\, e^{-\frac{k\beta}{\alpha}\left[1+\left(1+\frac{2f^2\alpha^2}{k^2 D^2 \sigma_M^2}\right)^{-1}\right]x_3 \omega'}\, e^{-\frac{1}{2\sigma_M^2\left(1+\frac{2f^2\alpha^2}{k^2 D^2 \sigma_M^2}\right)}(f\beta\omega' - \xi')^2} \tag{152}$$

Describing a_{in} in the time domain:

$$\propto \int_{-\infty}^{\infty} d\Omega\, h(\Omega' - \Omega) \int_{-\infty}^{\infty} dt\, e^{i\Omega t}\, \chi_{ijk}^{(2)}(t; t', t')\, |E_{out}(x_3, t')|^2\, e^{-\frac{(\xi - \xi')^2}{2\sigma_M^2}}$$

$$+ \int_{-\infty}^{\infty} d\Omega\, h(\Omega' - \Omega) \int_{-\infty}^{\infty} dt'\, e^{i\Omega t'}\, \chi_{ijk}^{(2)}(t'; \tau, \tau')\, e^{-\frac{2\left(\frac{k\sigma_M}{\alpha f}\right)^2 x_3^2 + i\left(\frac{2k}{\alpha f}\right)x_3(\xi - \xi')}{\left(\frac{k^2 D^2 \sigma_M^2}{f^2 \alpha^2} + 2\right)}}$$

$$\times \int_{-\infty}^{\infty} a_{in}(\tau)\, d\tau \int_{-\infty}^{\infty} d\omega\, e^{i\omega\left\{\tau - t' - \frac{k\beta}{\alpha}\left[1+\left(1+\frac{2f^2\alpha^2}{k^2 D^2 \sigma_M^2}\right)^{-1}\right]x_3\right\}}\, e^{-\frac{1}{2\sigma_M^2\left(1+\frac{2f^2\alpha^2}{k^2 D^2 \sigma_M^2}\right)}(f\beta\omega - \xi)^2}$$

$$\times \int_{-\infty}^{\infty} a_{in}^*(\tau')\, d\tau' \int_{-\infty}^{\infty} d\omega'\, e^{-i\omega'\left\{\tau' - t' - \frac{k\beta}{\alpha}\left[1+\left(1+\frac{2f^2\alpha^2}{k^2 D^2 \sigma_M^2}\right)^{-1}\right]x_3\right\}}\, e^{-\frac{1}{2\sigma_M^2\left(1+\frac{2f^2\alpha^2}{k^2 D^2 \sigma_M^2}\right)}(f\beta\omega' - \xi')^2} \tag{153}$$

Perform the integration over ω and ω'

$$\propto \int_{-\infty}^{\infty} d\Omega\, h(\Omega' - \Omega) \int_{-\infty}^{\infty} dt\, e^{i\Omega t}\, \chi_{ijk}^{(2)}(t; t', t')\, |E_{out}(x_3, t')|^2\, e^{-\frac{(\xi - \xi')^2}{2\sigma_M^2}}$$

$$+ \int_{-\infty}^{\infty} d\Omega\, h(\Omega' - \Omega) \int_{-\infty}^{\infty} dt'\, e^{i\Omega t'}\, \chi_{ijk}^{(2)}(t'; \tau, \tau')\, e^{-\frac{2\left(\frac{k\sigma_M}{\alpha f}\right)^2 x_3^2 + i\left(\frac{2k}{\alpha f}\right)x_3(\xi - \xi')}{\left(\frac{k^2 D^2 \sigma_M^2}{f^2 \alpha^2} + 2\right)}} \tag{154}$$

$$\times \int_{-\infty}^{\infty} a_{in}(\tau)\, d\tau\, e^{\frac{i\xi}{f\beta}\left\{\tau - t' - \frac{k\beta}{\alpha}\left[1+\left(1+\frac{2f^2\alpha^2}{k^2 D^2 \sigma_M^2}\right)^{-1}\right]x_3\right\} - \frac{\sigma_M^2}{2f^2\beta^2}\left(1+\frac{2f^2\alpha^2}{k^2 D^2 \sigma_M^2}\right)\left\{\tau - t' - \frac{k\beta}{\alpha}\left[1+\left(1+\frac{2f^2\alpha^2}{k^2 D^2 \sigma_M^2}\right)^{-1}\right]x_3\right\}^2}$$

$$\times \int_{-\infty}^{\infty} a_{in}^*(\tau')d\tau' \, e^{-\frac{i\xi}{f\beta}\left\{\tau'-t'-\frac{k\beta}{\alpha}\left[1+\left(1+\frac{2f^2\alpha^2}{k^2D^2\sigma_M^2}\right)^{-1}\right]x_3\right\}-\frac{\sigma_M^2}{2f^2\beta^2}\left(1+\frac{2f^2\alpha^2}{k^2D^2\sigma_M^2}\right)\left\{\tau'-t'-\frac{k\beta}{\alpha}\left[1+\left(1+\frac{2f^2\alpha^2}{k^2D^2\sigma_M^2}\right)^{-1}\right]x_3\right\}^2}$$

Having $\sigma_M \to 0$

$$G^2(x_3,\xi,\xi',\Omega') \to \int_{-\infty}^{\infty} d\Omega \, h(\Omega'-\Omega) \int_{-\infty}^{\infty} dt \, e^{i\Omega t} \, \chi_{ijk}^{(2)}(t;t',t')|E_{out}(x_3,t')|^2 \delta(\xi-\xi')$$

$$+ \int_{-\infty}^{\infty} d\Omega \, h(\Omega'-\Omega) \int_{-\infty}^{\infty} dt' \, e^{i\Omega t'} \, \chi_{ijk}^{(2)}(t';\tau,\tau')e^{-i\left(\frac{k}{\alpha f}\right)x_3(\xi-\xi')} \tag{155}$$

$$\times \int_{-\infty}^{\infty} a_{in}(\tau)d\tau \, e^{\frac{i\xi}{f\beta}\left(\tau-t'-\frac{k\beta}{\alpha}x_3\right)} \int_{-\infty}^{\infty} a_{in}^*(\tau')d\tau' \, e^{\frac{i\xi}{f\beta}\left(\tau'-t'-\frac{k\beta}{\alpha}x_3\right)}$$

We perform the integration over τ and τ'

$$\propto \int_{-\infty}^{\infty} d\Omega \, h(\Omega'-\Omega) \int_{-\infty}^{\infty} dt \, e^{i\Omega t} \, \chi_{ijk}^{(2)}(t;t',t')|E_{out}(x_3,t')|^2 \delta(\xi-\xi')$$

$$+ \int_{-\infty}^{\infty} dt' \, e^{i\Omega t'} \, e^{-i\left(\frac{k}{\alpha f}\right)x_3(\xi-\xi')} \chi_{ijk}^{(2)}\left(t';\frac{\xi}{f\beta},\frac{\xi'}{f\beta}\right) a_{in}\left(\frac{\xi}{f\beta}\right) a_{in}^*\left(\frac{\xi'}{f\beta}\right) \int_{-\infty}^{\infty} d\Omega \, h(\Omega'-\Omega) \, e^{-\frac{i(\xi-\xi')}{f\beta}t'} \tag{156}$$

We perform a Fourier transform back to the frequency domain:

$$G^2(x_3,\xi,\xi',\Omega') \propto \int_{-\infty}^{\infty} d\Omega \, h(\Omega'-\Omega) \int_{-\infty}^{\infty} dt \, e^{i\Omega t} \, \chi_{ijk}^{(2)}(t;t',t')|E_{out}(x_3,t')|^2 \delta(\xi-\xi')$$

$$+ e^{-i\left(\frac{k}{\alpha f}\right)x_3(\xi-\xi')} \chi_{ijk}^{(2)}\left(\Omega;\frac{\xi}{f\beta},\frac{\xi'}{f\beta}\right) a_{in}\left(\frac{\xi}{f\beta}\right) a_{in}^*\left(\frac{\xi'}{f\beta}\right) \int_{-\infty}^{\infty} d\Omega \, h(\Omega'-\Omega) \, \delta\left(\Omega-\frac{(\xi-\xi')}{f\beta}\right) \tag{157}$$

; and for the mirrored term

$$e^{i\left(\frac{k}{\alpha f}\right)x_3(\xi-\xi')} \chi_{ijk}^{(2)}\left(\Omega;\frac{\xi}{f\beta},\frac{\xi'}{f\beta}\right) a_{in}\left(\frac{\xi}{f\beta}\right) a_{in}^*\left(\frac{\xi'}{f\beta}\right) \int_{-\infty}^{\infty} d\Omega \, h(\Omega'-\Omega) \, \delta\left(\Omega+\frac{\xi-\xi'}{f\beta}\right) \tag{158}$$

The compete G2 result is:

$$G^2(x_3,\xi,\xi',\Omega') \propto \int_{-\infty}^{\infty} d\Omega \, h(\Omega'-\Omega) \int_{-\infty}^{\infty} dt \, e^{i\Omega t} \, \chi_{ijk}^{(2)}(t;t',t')|E_{out}(x_3,t')|^2 \delta(\xi-\xi')$$

$$+ e^{-i\left(\frac{k}{\alpha f}\right)x_3(\xi-\xi')} \chi_{ijk}^{(2)}\left(\Omega;\frac{\xi}{f\beta},\frac{\xi'}{f\beta}\right) a_{in}\left(\frac{\xi}{f\beta}\right) a_{in}^*\left(\frac{\xi'}{f\beta}\right) \int_{-\infty}^{\infty} d\Omega \, h(\Omega'-\Omega)\delta\left(\Omega-\frac{(\xi-\xi')}{f\beta}\right) \tag{159}$$

$$+ e^{i\left(\frac{k}{\alpha f}\right)x_3(\xi-\xi')} \chi_{ijk}^{(2)}\left(\Omega;\frac{\xi}{f\beta},\frac{\xi'}{f\beta}\right) a_{in}\left(\frac{\xi}{f\beta}\right) a_{in}^*\left(\frac{\xi'}{f\beta}\right) \int_{-\infty}^{\infty} d\Omega \, h(\Omega'-\Omega) \, \delta\left(\Omega+\frac{\xi-\xi'}{f\beta}\right)$$

If the bucket detector is a measure of complex phase for a specific generated frequency (Ω) that corresponds to a frequency difference between two spatially separated frequencies then the resulting corresponding complex phase will be the complex phase difference between the two spatially separated frequencies plus two additional phases: the phase induced by a spatial separation caused by the grating $\left(e^{i\left(\frac{k}{\alpha f}\right)x_3(\xi-\xi\prime)}\right)$ and the phase induced by the nonlinear condition $\chi_{ijk}^{(2)}\left(\Omega;\frac{\xi}{f\beta},\frac{\xi\prime}{f\beta}\right)$. Note this is provided that the nonlinear condition $\chi_{ijk}^{(2)}\left(\Omega;\frac{\xi}{f\beta},\frac{\xi\prime}{f\beta}\right)$ is met for the generation of the new frequency (Ω). A few questions arise from these results. Under what conditions is this achievable? How does one achieve a complex valued frequency-based bucket detector measurement? These questions will be addressed in the next chapter.

Chapter 5

5.   Complex Phase Measurement in a Terahertz Spectroscopy System

Two questions on the implementation of group delay ghost imaging arises from the analysis presented in the previous chapter. How can a complex valued frequency-based bucket detector measurement be taken and under what conditions will the nonlinear condition be satisfied to achieve difference frequency generation? Both questions are easily answered and satisfied with the use of a Terahertz Time-Domain Spectroscopy (THz-TDS) system. We will first look at one of many Terahertz Time-Domain Spectroscopy (THz-TDS) system and how it functions and in doing so it will be shown how complex valued frequency-based measurements are routinely made in a THz-TDS system. Then the appropriate nonlinear conditions will be described that will satisfy the conditions for group delay ghost imaging performed by a slight adjustment of the THz-TDS system along with a given scenario in which frequency difference ghost imaging can be implemented.

5.1   Terahertz Time-Time Domain Spectroscopy setup

There are many ways in which a freely propagating THz pulse can be generated. There are also numerous ways in which the THz pulse can be measured. A given THz-TDS system can be seen in figure 9 [56].
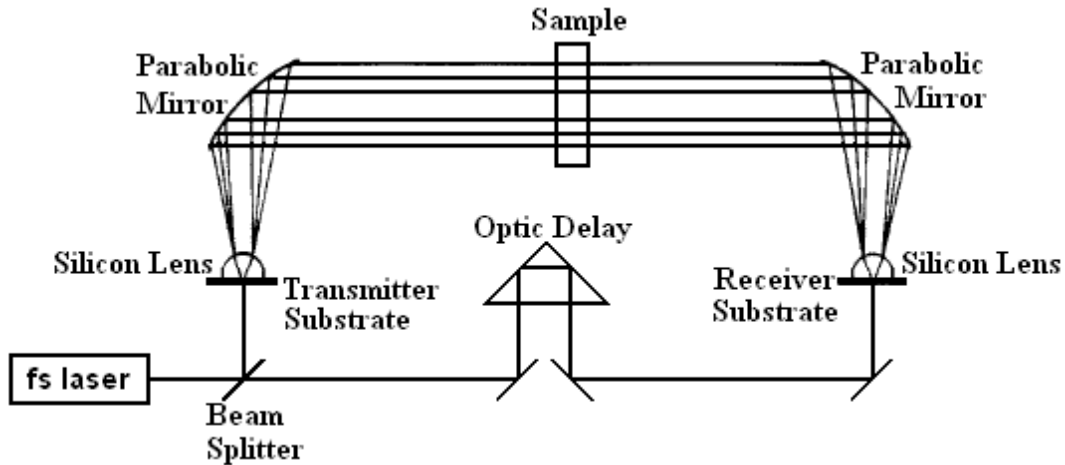
Figure 10: An example of a terahertz time domain spectroscopy system [56].

In this THz-TDS system the femtosecond (fs) laser is a mode locked Ti-sapphire laser that has a repetition rate around 85MHz. The operating center wavelength of the laser is around 810nm. The emitted pulses from the fs-laser are first incident upon the beam splitter in which half of the pulse travels on to the transmitter while the other half travels through an optic delay line to the receiver. In this setup the transmitter is comprised of two 10μm wide aluminum lines spaced 80μm apart on a gallium arsenide (GaAs) substrate. A voltage is applied across the two aluminum transmission lines of about 80V, which slightly less than the ionization break down voltage of air. When the incident optical pulse from the femto-second laser creates electron-hole pairs in the GaAs substrate the now free electrons (and to a lesser degree, holes) undergo ballistic acceleration. THz radiation is generated due to this ballistic acceleration. On the other side of the GaAs substrate is a truncated high resistivity silicon lens. The silicon lens is used to direct the THz radiation to the first parabolic mirror in figure 9. This parabolic mirror is used to collimate the THz pulse. Once collimated, the THz pulse interacts with a sample material, which is placed in the center of the THz system. After passing through the sample the THz pulse is incident upon the second parabolic mirror. The second parabolic mirror is used to re-image the THz pulse onto

57

the receiver. To further focus down the THz pulse onto the receiver a silicon lens is placed onto

the receiver substrate. The receiver is comprised of two 10μm wide aluminum transmission lines

spaced 50μm apart with two extruding aluminum blocks between the transmission lines. A

schematic of the receiver can be seen in figure 10.
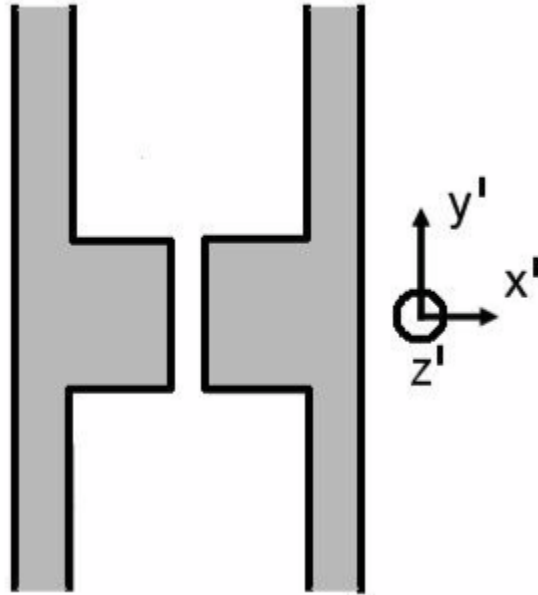
Figure 11: A schematic of a THz receiver transmission lines.

The two receiver transmission lines are on a highly ion implanted silicon on sapphire substrate.

The optically delayed pulse from the fs-laser frees electrons in the silicon on sapphire substate in

between the two transmission lines, while the incident terahertz pulse creates an electric field,

which drives a current between transmission lines. There must be both free electrons and an

electric field to have a current. If one or the other does not exist no current will be generated. A

current amplifier then amplifies this current. The resulting amplified current is proportional to the

electric field of the THz pulse. The detection of a THz pulse can be described by the following

three equations:

$$g(t) = \int_{-\infty}^{t} I(t')e^{-\frac{(t-t')}{\tau_c}} dt' \qquad (160)$$

$$V(t) = \int_{-\infty}^{t} E(t')e^{-\frac{(t-t')}{Cz_0}} dt' \qquad (161)$$

$$Q(\tau) = \int_{-\infty}^{\infty} g(t' - \tau)V(t')dt' \qquad (162)$$

where $I(t')$ is the laser pulse, τ_c is the carrier lifetime, C is the capacitance of the transmission line gap, and z_0 is the transmission line impedance. The measured current $(Q(\tau))$ is a convolution, in the temporal domain, between the voltage $(V(t))$, generated by the THz pulse $(E(t'))$, and the freed electron-hole pairs $(g(t))$, generated by the femtosecond optical pulse $(I(t'))$. The measured current $(Q(\tau))$ would be a faithful representation of the THz pulse $(E(t'))$ if not for the frequency-dependent term of the autocorrelation of the probing pulse $(g(t))$ which in turn is the laser pulse $(I(t'))$. This frequency-dependent term has little effect when the bandwidth of the probing pulse is much larger than the bandwidth of the THz pulse. A temporal visual picture of this can be seen in figure 11.
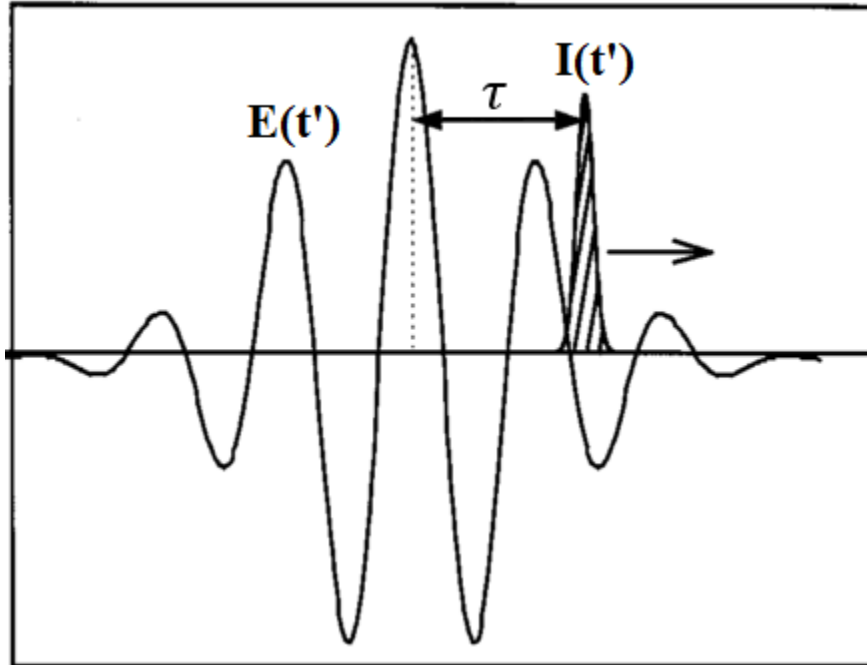
Figure 12: A temporal picture of the THz pulse $E(t')$ being convolved with a probing pulse $I(t')$ in the detection of a THz pulse [31].

When the bandwidth of the integrating optical pulse $\left(I(t')\right)$ is much larger than the bandwidth of the THz pulse $\left(E(t')\right)$ the temporal features of the THz pulse can be seen because the temporal duration of the optical pulse is much smaller than that of the THz pulse. For the usual experimental situation regarding THz spectroscopy this is easily satisfied because the bandwidth of the optical pulse is much greater than the carrier frequency of the THz pulse.

With the qualifications stated aforementioned, the traditional data analysis of a THz spectroscopy system is a measurement of the complex refractive index as a function of frequency. To increase the signal to noise ratio, of the measured current, a lock-in amplifier with a mechanical chopper are used to enhance the measurement of the resulting current/electric field amplitude as a function of optical delay. A mechanical chopper modulates the THz signal passing to the receiver. The resulting complex field is plotted as a function of time/optic delay. It is the Fourier transform of this electric field that gives the complex field as a function of frequency.

$$F(\Omega) = \int_{-\infty}^{\infty} f(t)e^{-i2\pi\Omega t}dt \tag{163}$$

A measurement of the complex field amplitude as a function of frequency is done for both a sample scan and a reference scan. A reference scan is a scan of a THz pulse without a sample inside of the system. The extraction of the effects of the sample on the THz pulse is found by taking the ratio between the reference scan and the sample scan.

$$F_{result}(\Omega) = \frac{F_{sample}(\Omega)}{F_{reference}(\Omega)} \tag{164}$$

Without the reference scan the effect the sample has on the THz pulse cannot be determined.

5.1.1 Transmitter

In the previous section, a THz pulse was generated from the ballistic acceleration of freed electrons by an ultrashort pulse incident between two transmission lines with a large DC voltage between them. This is by no means the only way of generating a THz pulse. One such way of generating a THz pulse is through difference frequency generation with the use of Gallium Phosphide (GaP). GaP has a large nonlinear optical coefficient and its phase-matching conditions are relatively easily satisfied for optical rectification in the collinear geometry [57]. If the GaP crystal is sufficiently thin, absorption caused by GaP on the optical pulse and the generated THz pulse can be neglected. An optical pulse can be well-detuned away from any resonances. Lastly the generated THz frequencies are well below the phonon resonances of GaP. This means that since the absorption and dispersion can be neglected, the nonlinear term χ_{ijk} does not depend on optical frequency.

Starting with an unknown ultrashort optical pulse incident upon a thin GaP crystal will generate a THz pulse through difference frequency generation. If the unknown optical pulse is

well detuned away from any resonances within GaP crystal, the nonlinear term χ_{ijk} will not depend on optical frequency. The resulting generated THz pulse's electric field can then be measured as a function of time through, essentially it is an autocorrelation between the THz pulse and the unknown optical pulse. The Fourier transform of the temporal THz pulse will give the complex field in the frequency domain. For a given realization, the complex field is the ratio between a sample (a given realization) and a reference. The reference is a THz pulse generated from the totality of the unknown optical pulse. It is then through a fourth order correlation between a given THz complex field value for a specific frequency and the corresponding optical frequencies that contribute to generate the specific THz frequency that the group delay for an unknown optical pulse can be determined. In the next chapter through numerical analysis for a given set of qualifying conditions that the group delay for an unknown optical pulse can be determined using difference frequency generated ghost imaging.

Chapter 6

6. Numerical Simulation

This chapter contains a numerical simulation of a second order correlation between the spatial configuration of the BSLM and the THz frequency measurement for an unknown optical pulse which is displayed in the frequency domain in figure 12. The discretized numerical simulation space will be based on three off the shelf components: lens, grating, and BSLM. The BSLM is the Texas Instruments DLP650LNIR, which is comprised of 1280 X 800 orthogonally placed micromirrors [58]. The distance between the center of each micromirror to its translational neighbor for this BSLM is 10.8μm. This BSLM is the physical representation of the mask function $M(\chi)$. Each of the 800 columns along the 1280- micromirrors axis is completely independent from all other columns and each column has an equal probability of being on or off for each realization. In this numerical simulation, the random mask function is represented by equation (100) and figure 7. The mask function is a 1280 length vector function with each element within the vector representing the state of a BSLM micromirror column for a given realization. The grating which is offered by Thor Labs is a 1200 grooves per mm reflective grating [59]. Using a 100mm focal length lens and by reviewing equation (135) we can determine the central frequency located on each micromirror.

$$E_{out}(x_3, \omega) = \int_{-\infty}^{\infty} a_{in}(\omega) e^{-i\frac{k\beta\omega}{\alpha}x_3} e^{-\frac{k^2 D^2 (f\beta\omega - \chi)^2}{4f^2\alpha^2}} e^{-i\frac{kx_3}{\alpha f}\chi} M(\chi) d\chi \qquad (165)$$

The central frequency occurs when $f\beta\omega - \chi = 0$. Using the distance between each micromirror (10.8μm) the focal length of the lens (100mm), and by calculating β using equation (125) we can determine the change in frequency between consecutive micromirrors. The ultrafast unknown optical pulse used in this numerical simulation will have a Gaussian amplitude in the frequency domain. The Gaussian distribution will have a full width half maximum (FWHM) of 5nm with a central wavelength of 805nm. In setting the central micromirror to 805nm the resulting spread of the unknown optical pulse across the BSLM is from 796nm to 814nm. Based on the above off the shelf components, the chosen unknown ultrafast optical pulse, and for ease of calculation for the Fourier transform the discretized simulation space will be 2048 pixels with a one to one conversion from the frequency domain to the BSLM micromirror spatial domain.
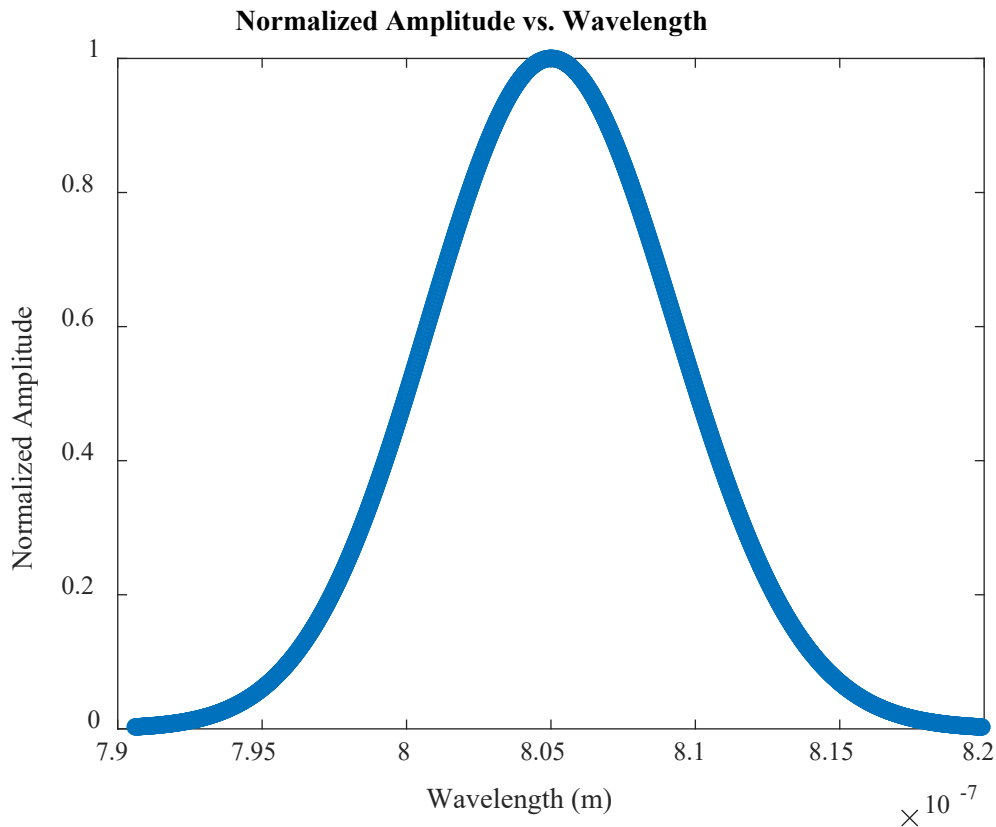

Figure 13: Spectral amplitude for the unknown optical pulse in the frequency domain.

This frequency domain representation of the incident unknown optical pulse extends over 2048 units with a frequency difference such that an individual frequency is centrally located on an BSLM micromirror if there is one. The spectral phase for this unknown optical pulse was given a parabolic shape with a range from 0 to 2π across the 2048 units. This spectral phase can be seen in figure 13.
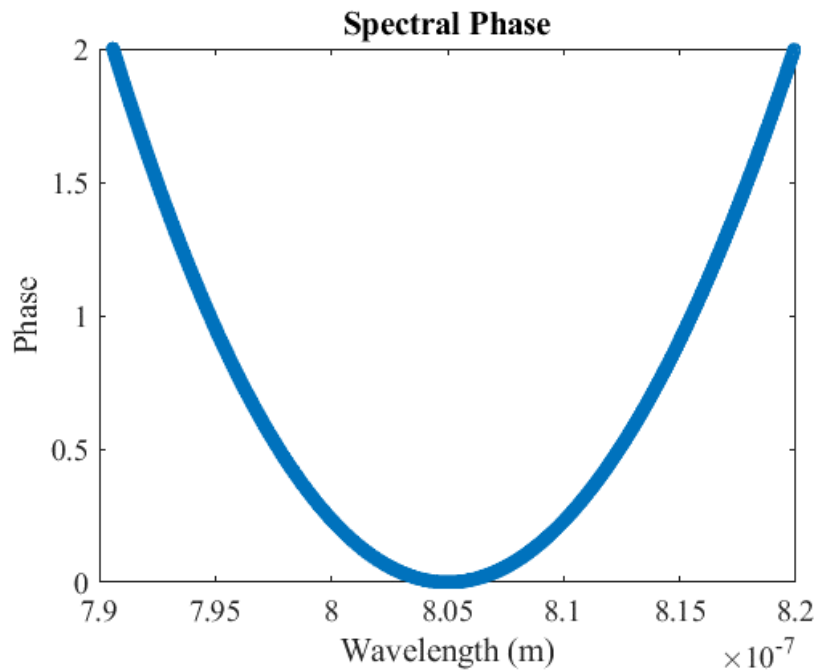
Figure 14: Spectral phase for the unknown optical pulse. The spectral phase was given a parabolic structure for the frequencies spanning across the BSLM.

Figures 12 and 13 show the frequency domain representation of amplitude and phase respectively for an unknown optical pulse extending from790nm to 820nm. When considering the BSLM the ends of the unknown pulse are truncated due to the lack a micromirror at that spatial location. Figures 14 and 15 show the resulting frequency domain representation of amplitude and phase respectively for an unknown optical pulse when the BSLM is considered along with the simulation space of this numerical simulation.

Figure 15: Spectral phase for the unknown optical pulse with the physical bounds of the BSLM considered.

Figure 16: Spectral phase for the unknown optical pulse with the physical bounds of the BSLM considered.

This unknown ultrafast optical pulse will generate a THz pulse when it passes through a sufficiently thin GaP crystal in the collinear geometry [57]. Using the abov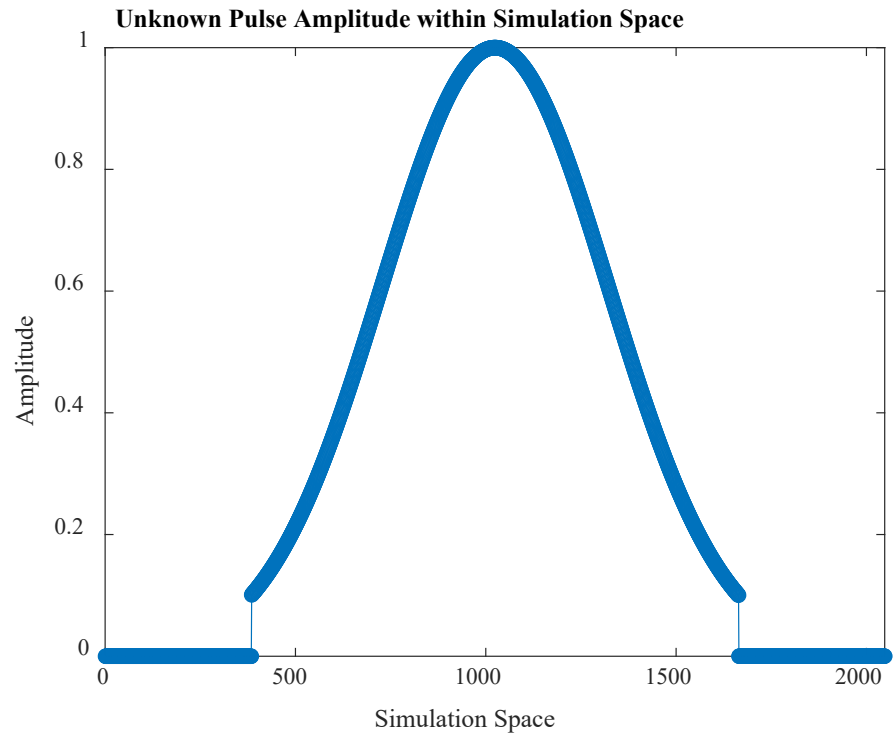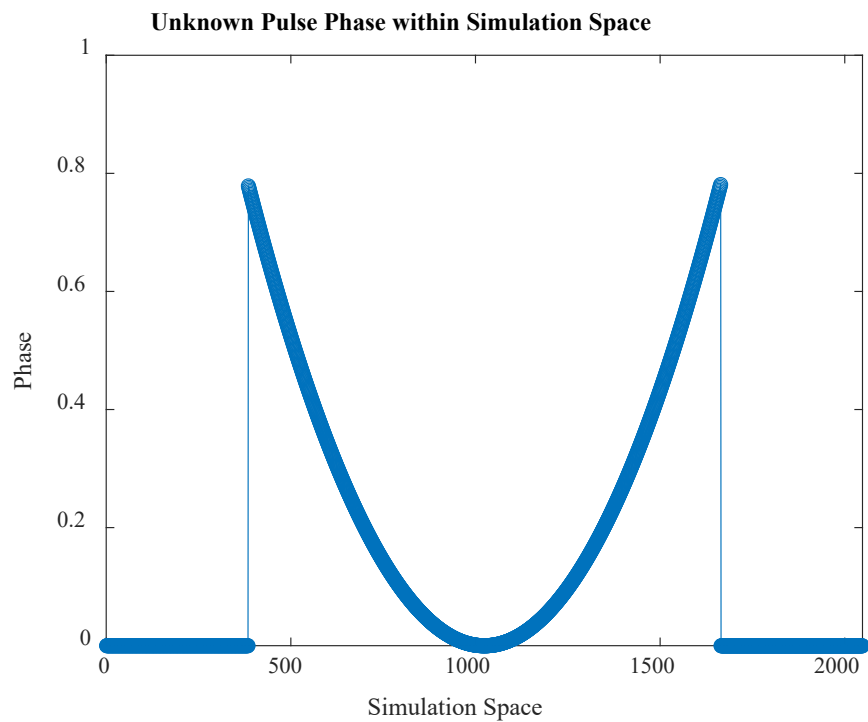e defined simulation space, the unknown ultrafast optical pulse described in the previous paragraph, and a given realization of the mask function we can numerically simulate the frequency domain of the unknown ultrafast optical pulse incident upon the nonlinear material through the use of equations (124), (125) and (135). When equation (135) is calculated for a given realization equation (136) can be calculated which will give the resulting THz pulse in the frequency domain. In relation to spatial ghost imaging for each realization there are two measurements: a spatially resolved field, and a bucket detector measurement. For this numerically simulated group delay frequency ghost image we also have two measurements: a complex valued THz pulse frequency domain measurement (bucket detector measurement) and a BSLM mask function matrix measurement. While it is the 1280 length mask function vector that depicts which frequencies of the unknown ultrafast optical pulse are passed by the BSLM, it is the 1280 X 1280 mask matrix (equivalent to the spatially resolved field measurement) that depicts the combination of the unknown ultrafast optical pulse frequencies that contribute to the generation of the complex valued THz pulse frequency domain measurement. As stated in chapter four the BSLM mask function matrix is determined by preforming matrix multiplication between the mask vector and its transpose. As I also showed in chapter four, table 1 each diagonal in this mask matrix corresponds to the generation of a different THz frequency through difference frequency generation. The bucket detector measurement is a complex value measurement of a THz frequency which corresponds to one of the diagonals along the mask matrix. Numerically this corresponds to one value in the vector calculation of equation (136). The difference between an experimental second order correlation and this numerical simulation is in an experiment the bucket detector must first measure

the generated THz pulse in the temporal domain through an autocorrelation between the generated THz pulse and an integrating optical pulse followed by a Fourier transform conversion from the temporal domain to the frequency domain to determine the complex valued THz frequency measurement.

The number of different realizations used in this numerical simulation was 20480. This number of realizations was chosen because this is 16 runs of 1280 realizations, with 1280 being the number of BSLM micromirrors. The measurement bucket detector frequency used in the simulation was 0.5 THz which corresponds to the 75th diagonal away from the central diagonal of the BSLM mask matrix. The resulting numerical simulated ghost imaging of phase difference for 0.5 THz along with the actual phase difference for 0.5 THz can be seen in figure 16.

Figure 17: A plot of the actual phase difference between frequencies of the unknown optical pulse with a frequency difference of 0.5 THz in red with the calculated second order correlation phase difference through numerical simulation of 20480 realizations in blue.

The vector length of the 75th diagonal is 1206 which corresponds to 1280 – 74. As it can be seen the ghost phase difference closely predicts the actual phase difference with regards to the central frequencies of the unknown ultrafast optical pulse. As we move away from the center of the group delay generated by the central frequencies of the unknown optical pulse the phase deference generated by ghost imaging deviates away from the actual phase difference.

In the previous simulation the total number of realizations was 20480 which corresponded to 16 runs of 1280 realizations. The realization number of 1280 corresponded to the total number of BSLM elements. From a practical standpoint the total number of realizations 20480 could be too many and as such we shall now perform another numerical simulation that reduces the scale of precision to reduce the total number of realizations. This will be done by grouping the 1280 BSLM elements into groups of 80. By doing this we transition from a 1280-length mask vector to a 16-length mask vector. The total number of runs for this configuration will be 256 which corresponded to 16 runs of 16 realizations. For the bucket detector measurement, we will shift from 0.5 THz which corresponded to the 75th diagonal to 0.53 THz which corresponded to the number of BSLM element grouped together and the 80th diagonal of the mask matrix. The resulting numerical simulated ghost imaging of phase difference for 0.53 THz along with the actual phase difference for 0.53 THz can be seen in figure 17.
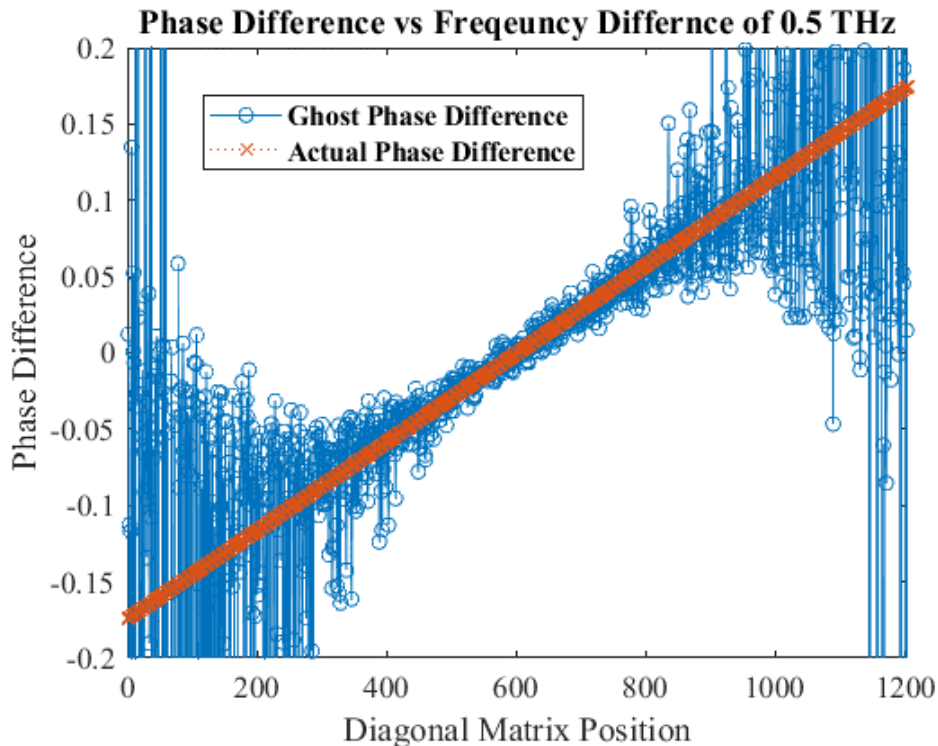
Figure 18: A plot of the actual phase difference between frequencies of the unknown optical pulse with a frequency difference of 0.53 THz in red with the calculated second order correlation phase difference through numerical simulation of 256 realizations in blue. This numerical simulation consists of grouping the 1280 BSLM elements into 16 groups of 80.

Here the vector length of the 80th diagonal is 1199 which corresponds to 1280 – 81. In this numerical simulation we again see greater accuracy in determining the phase difference with regards to the central frequencies compared to the tail frequencies. The simplest way to increase the accuracy of phase difference through ghost imaging is to increase the total number of realizations which can be directly seen in figure 18.
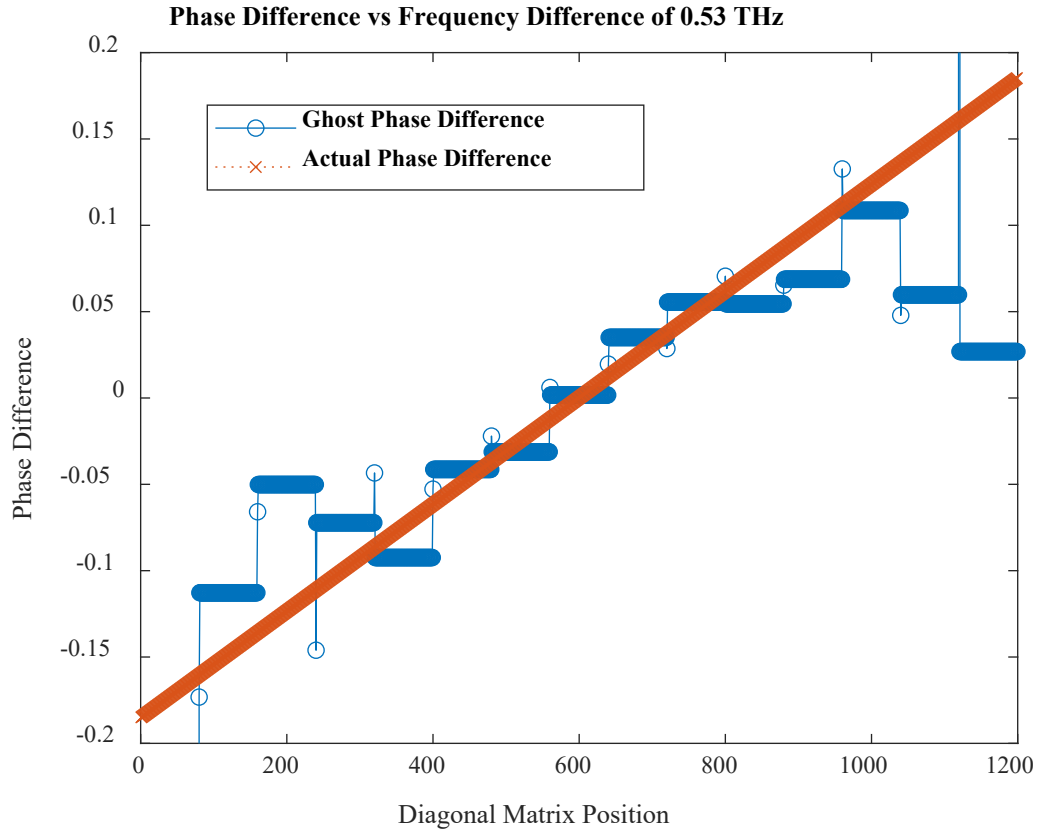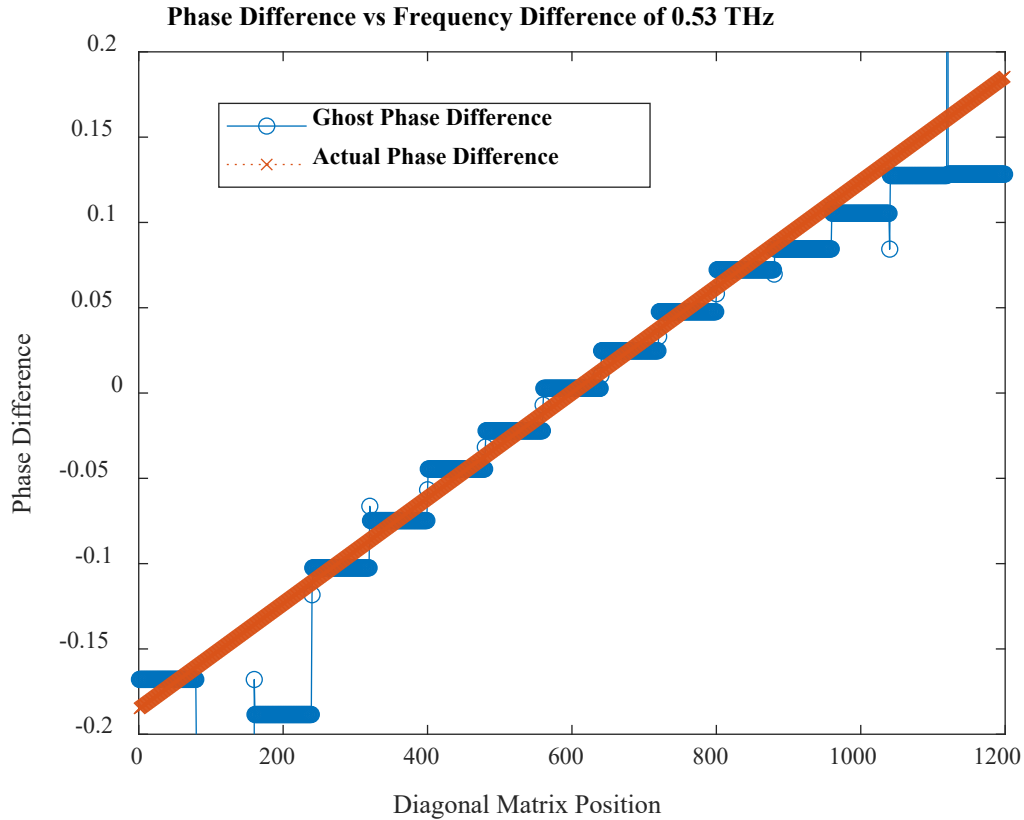
Figure 19: A plot of the actual phase difference between frequencies of the unknown optical pulse with a frequency difference of 0.53 THz in red with the calculated second order correlation phase difference through numerical simulation of 2560 realizations in blue. This numerical simulation consists of grouping the 1280 BSLM elements into 16 groups of 80.

As in the previous numerical simulation there are 16 groups of 80 BSLM elements with the bucket detector measurement of 0.53 THz for each realization. The total number of realizations this time was increased by a factor of ten going from 256 to 2560. It is quite evident when comparing figure 17 to figure 18 that as the number of realizations increases the accuracy with regards to phase difference using ghost imaging increases and the accuracy of phase difference falls the further, we travel from the central frequencies.

Chapter 7

7.   Comparison with Other Group Delay Measuring Methods

The focus of the comparison will be on errors in the FROG technique. The errors are of two varieties: sampling errors and noise errors. Lacking a proper sampling rate and not containing all sampling data within the FROG-trace grid will result in mischaracterization of the unknown optical pulse. Noise errors come in two varieties multiplicative and additive. We will first look at the sampling error followed by the noise errors.

7.1   FROG error

If a signal that is band-limited is sampled at a rate at least as high as the Nyquist rate given the Nyquist criterion it contains all required information regarding that signal [60]. Sampling at a higher rate than the Nyquist produces no additional information, without noise considerations. The Nyquist rate requires sampling to be at least twice as high as the highest frequency in a signal. However, the FROG sampling rate (FSR) has a stricter criterion than the Nyquist rate. If a signal is sampled at the Nyquist rate as opposed to the FSR, there will be truncated data that will not fall upon the FROG-trace grid. There are two limits that FSR is required to satisfy [61]. The first is that the temporal step Δt does not extend off the FROG-trace grid in the frequency direction. This temporal step is satisfied by the following:

$$\Delta t \leq \frac{1}{6.3 f_p} \approx \frac{\lambda_0^2}{6.3 c \lambda_p} \tag{166}$$

where λ_0 is being the central wavelength and $\lambda_p \left(f_p \right)$ is being the FWHM of the spectrum. For a bandwidth limited pulse, the required minimum sampling time ratio is: $t_p / \Delta t \geq 2.78$ with t_p being the FWHM of the pulse temporal width. While this is the first FSR sampling step size limit, FROG has a second one that prevents the FROG-trace data so that it does not extend off the grid in the time-delay direction. For a Gaussian pulse this limit is the following:

$$\Delta t \geq \frac{4.5 t_p}{N} \tag{167}$$

where N is the grid size for the FROG-trace. while the above step size limits were calculated for Gaussian pulses, other pulses and spectral shapes will have different FSR limits. A FROG trace must satisfy both equations (166) and (167) to capture all significant temporal data and contain it within the FROG-trace grid. If either is not satisfied the FROG-trace will lack information about the unknown pulse.

Experimental measurements of the FROG-trace are performed by a CCD camera. FROG noise arises from the use of an imperfect detectors. The error could be multiplicative or additive [62]. Multiplicative noise is less detrimental to recovering the unknown optical pulse, because it only affects the part of the FROG trace that has a measured quantity. If multiplicative error is 10% in noise trace results in only 1% rms error in the retrieved pulse intensity and phase [62]. This multiplicative noise arises from the pixel-to-pixel signal variations that are proportional to the intensity measured at a pixel.

On the other hand, additive error is harder to compensate for because unlike multiplicative error it affects the entire FROG-trace. This error arises from pixel-to-pixel signal variations independent

of the FROG intensity at a given pixel. An example of additive error is thermal noise that occur in CCD cameras. A 10% additive noise means there is a 10% noise everywhere in the FROG-trace. It is only in using noise filtering techniques that there will be only a 1% rms error in the retrieved pulse intensity and phase.

7.2 SPIDER error

For SPIDER technique, the spectral phase of the unknown pulse is encoded in the fringe spacing of the generated interferogram. This interferogram is generated by taking an unknown pulse and passing it through a beam splitter to create unknown pulse A and unknown pulse B. Unknown split pulse A is then passed through a dispersive material to broaden it. Unknown pulse B is unmodified, and it travels a variable length optical path. A trace between modified unknown pulse A and unknown pulse B is performed in a sum frequency generated in a nonlinear material to create a spectral shear between the two unknown pulses. The sum is measured by a spectrometer to create spectrograph is created. Recovery of the group delay using SPIDER is of the following:

$$GD(\omega_c) = \frac{\partial \phi}{\partial \omega}|_{\omega_c} \approx \frac{\phi(\omega_c + \Omega) - \phi(\omega_c)}{\Omega} \tag{168}$$

The chosen spectral shear (Ω) of the SPIDER technique determines the step size of the recovered group delay. It is critical in SPIDER that the wavelength calibration of the spectrometer be performed, because even the smallest wavelength calibration error can generate significant measurement error [63]. For a wavelength calibration error of ϵ_λ this corresponds to a misestimation of the group delay of:

$$\epsilon_{GD} = \frac{\omega}{\Omega} \tau \frac{\epsilon_\lambda}{\lambda} = \frac{2\pi c}{\lambda} \beta_2 l \frac{\epsilon_\lambda}{\lambda} \tag{169}$$

where β_2 is dispersion and l is the length of dispersive material. As an example, for a miscalibration of 0.01 nm this generates a group delay error of about 0.5 femtoseconds. Another error in SPIDER is detection error which is unrelated to calibration error. The spectral shear Ω between the two unknown pulse cannot be made arbitrarily small because detection noise dominates over the actual phase difference. On the other hand, $\partial\omega$ cannot be made to large for it sacrifices spectral resolution.

7.3 MIIPS error

To measure group delay, MIIPS introduces a well-known reference function $f(\omega)$ with the use of a pulse shaper to locally cancel the distortions by the unknown spectral phase $\phi(\omega)$ of the unknown pulse. A commonly used pulse shaper is a combination of a frequency spreader and a phase only spatial light modular (POSLM). The POSLM imparts an additional phase on $\phi(\omega)$ corresponding to the frequency incident upon each pixel of the POSLM. This new pulse has a new phase and it is given by $\varphi(\omega) = \phi(\omega) + f(\omega)$. A second harmonic generation (SHG) is then used to retrieve the unknown phase $\phi(\omega)$. Retrieval of $\phi(\omega)$ is given by the two following equations [64]:

$$I(2\omega) = \left| \int |E(\omega + \Omega)||E(\omega - \Omega)|e^{i[\phi(\omega+\Omega)+\phi(\omega-\Omega)]}d\Omega \right|^2 \qquad (170)$$

$$\phi(\omega + \Omega) + \phi(\omega - \Omega) = 2\phi(\omega) + \phi''^{(\omega)\Omega^2} + \frac{2}{(2n)!}\phi^{2n\prime}(\omega)\Omega^{2n} + \cdots \qquad (171)$$

where on the right side of equation (171) is a Taylor series expanded around ω. When $\phi(\omega + \Omega) + \phi(\omega - \Omega)$ is zero, maximal generation of the second harmonic signal occurs. This equivalently takes place when $\phi''^{(\omega)} = -f''(\omega)$. By scanning $f(\omega)$ across the spectrum of the unknown pulse,

$\phi(\omega)$ can be determined. Due to Taylor expansions around $\phi(\omega)$ and $f(\omega)$, some systematic error occurs. For example when the well-known reference function is: $f(\delta, \omega) = \alpha \sin(\gamma\omega - \delta)$ is used with δ being phase shift, α being a fixed parameter with value 1.5π, and γ also being a fixed parameter equal to the duration of the pulse this error for the second derivative of $f(\omega)$ is calculated as $1/12\gamma^2/\tau_0^2$ where τ_0 is the time duration of the pulse. A single scan of the pulse error is $\sim 10\%$ when $\gamma^2/\tau_0^2 \approx 1$. The sum of all errors from all nonlinear terms of $\phi(\omega)$ which define the error in the second derivative of the measured phase is:

$$\phi''_{measured} \approx \phi'' \left(1 \pm \sum_n \frac{\phi^{n'}}{\tau_0^{2-n} n!} \right) \tag{172}$$

Two additional notes are due regarding this error. MIIPS factorially decreases the error every iteration. The error is greatest on the spectral sidelobes of the pulse.

Aside from the error resulting from the Taylor expansion there is also error with regards to digital noise of the retrieved ϕ''. This error is equal to $4\pi\alpha\gamma^2/N$ where N is being the number of steps in the scan. The smallest possible phase delay that the POSLM can provide along with the number of pixels being used determine the lower limit of the step size. Using a POSLM with a greater number of pixels yields better accuracy when a smaller step size is used.

7.4 Summary of errors among various techniques

Each technique, be it FROG, SPIDER, MIIPS or the one proposed in this dissertation which I will call group delay via frequency ghost imaging (GD-FGI) has error associated with its determination of group delay. While each method contains errors and those errors fall under two categories: those that can be mitigated and those that may not. Errors that can be mitigated are

ones such as measurement error, optical alignment, and use of optical material choices. Errors that

currently hard to mitigate are ones that cannot be minimized through various means of suppression.

Error with regards to GD-FGI in viewing equation (159) in chapter 4 error arises in two forms:

the size of the matrix, and the ghost imaging technique. increasing the discretization of the matrix

will yield a better approximation of group delay but at the cost of needing to have more realizations

for an accurate group delay approximation. In the following table is a breakdown of errors

associated with each technique.

Table 2: Technique along with their corresponding associated errors.

Technique	Mitigatable Error	Unmitigable Error
FROG	CCD measurement noise (thermal)	Not satisfying the FROG sampling rate (FSR)
SPIDER	Chosen spectral shear	Miscalibration of spectrometer
MIIPS	Spatial discretization of the POSLM	n number of steps in a scan
DG-FGI	Spatial discretization of the BSLM	n number of realizations

Chapter 8

8. Conclusion

The temporal duration of an optical pulse is determined by two factors: spectral bandwidth and spectral phase. While the measurement for determining spectral bandwidth is relatively easy for any temporal size, long or short, the measurement for determining spectral phase becomes increasingly difficult to impossible as temporal duration decreases. When it is impossible to determine, the spectral phase of an optical pulse methods have been developed to determine the group delay of the optical pulse. Group delay being the derivative of spectral phase with respect to frequency. These methods include frequency resolved optical gating (FROG), spectral phase interferometry for direct electric-field reconstruction (SPIDER), and multiphoton intrapulse interference phase scan (MIIPS). Each of the named methods generate a new frequency which contains information regarding the group delay through a nonlinear process that uses a nonlinear optical material. New frequency generation is the result of frequency mixing taking the form of frequency doubling, sum frequency generation, difference frequency generation and optical rectification. FROG, SPIDER, and MIIPS use either doubling or sum frequency generation. Optical rectification and Difference frequency generation have not been used to determine the group delay of an unknown optical pulse. In this dissertation it is shown how in combination of correlated imaging and difference frequency generation can determine the group delay of an unknown ultrafast optical pulse.

This dissertation has taken a methodical approach to show how the group delay of an unknown ultrafast optical pulse can be determined using correlated imaging and difference frequency generation. To show this we began in chapter one by laying the mathematical background by describing the wave nature of light. At the start of chapter one we begin with a mathematical description of a monochromatic time dependent wave, originating from the wave equation. It is from this description that we contextualize a waves amplitude, phase, and often measured intensity. Next, we mathematically describe a plane wave which is the inclusion of an additional dependent variable, space. In doing so we can make a distinction between a wave traveling through free space and a wave traveling through some material. To continue expanding on the mathematical description of the wave nature of light the Fourier transform is introduced so we can expand from a monochromatic traveling wave to a polychromatic traveling wave. We now see that spectral phase is a function of phase versus frequency for a polychromatic wave with the derivative of spectral phase being group delay. Likewise, we see that if we know group delay for a polychromatic wave then the integral of group delay is the spectral phase for the polychromatic wave plus some constant phase term across the spectrum. It is here we end our mathematical background description on the wave nature of light.

Chapter two begins with Maxwell's four in order to describe what happens when a monochromatic wave travels through a nonlinear optical material. In using an anharmonic oscillator model approach to describe the nonlinear optical material response and looking at the second order susceptibility we see that there are four possible outcomes: second harmonic generation (SHG), sum frequency generation (SFG), difference frequency generation (DFG), and optical rectification (OR). Upon further examination of DFG with the use of two monochromatic

waves we see that the resulting initial phase of the newly generated frequency is equal to the phase difference between the two monochromatic fields. We then expand upon this by seeing what the resulting initial spectral phase of a difference frequency generated polychromatic wave when for two polychromatic sources are used. What we find is that the initial phase for a frequency generated by DFG is an integral sum of phase differences between the two polychromatic sources that have a frequency difference equal to newly generated frequency. Normally, even though the spectral phase of the newly generated polychromatic wave can be determined, it contains zero information about spectral phase of the generating polychromatic sources. It is here we bring in correlated imaging (aka ghost imaging) to gain information regarding the spectral phase of the polychromatic sources.

Chapter three begins by introducing correlated imaging (aka ghost imaging). This is done through giving a brief history of ghost imaging from generating a spatially resolved ghost image using orthogonally polarized signal and idler beams created by a type-II phase-matched spontaneous parametric down-conversion (SPDC) [26] to generate a spatially resolved ghost image using the cross-correlation measurements made by two detectors with non-entangled source fields. The resulting cross-correlation measurements can either be phase-sensitive or phase-insensitive. Through the history of spatial ghost imaging there are two key measurements: bucket detector and spatially resolved field. It is the cross-correlation between these two measurements that generate a ghost image. The rest of chapter three involves the generation of a resolved field for the use one of the many realizations used to generate a ghost image.

Chapter four constitutes the merging of ghost imaging and DFG to show how the group delay for an unknown optical pulse can be determined. However, before the merge between ghost

imaging and DFG can occur we looked at the second order correlation between the fundamental theorem of calculus and a random mask function. What we end up with is the original function with a change of variable pulse the mean value of an integral, multiplied by the average value of the random mask function. It is here that it is recognized that if a mask function was placed upon a polychromatic source used in DFG that the group delay of the polychromatic source can be determined by using ghost imaging. This was first shown qualitatively and then it is shown analytically through a fourth order correlation between two mask functions and the corresponding source frequencies. However, before a fourth order correlation was calculated a full accounting of all possible optical components used in an actual experiment that could impact phase needed to be considered. The optical components include grating, lenses, nonlinear optical material, and free space propagation. When the fourth order analytical calculation was completed, equation (159), we saw that if the bucket detector is a measure of complex phase for a specific generated frequency which corresponds to a frequency difference between two spatially separated frequencies then the resulting corresponding complex phase will be the complex phase difference between the two spatially separated frequencies plus two additional phases: the phase induced by a spatial separation caused by the grating and the phase induced by the nonlinear material. This is provided that the nonlinear condition is met for DFG as determined by the nonlinear material.

While chapter four was the analytical calculation of the fourth order correlation that resulted from merging of ghost imaging with DFG, chapter five outlined a scenario in which an experiment could physically take place and chapter six was a numerical simulation of such an experiment. An 805nm central wavelength with a 5nm full width half maximum optical pulse incident upon sufficiently thin GaP crystal in the collinear geometry will generate a THz pulse.

Using a THz spectroscopy set up as outlined in chapter five the resulting THz pulse electric field is measured in the temporal domain by completing an autocorrelation between the THz pulse and the unknown optical pulse. This temporal domain pulse is then Fourier transformed to the frequency domain for the complex phase bucket detector measurement for a realization. In completing this for many different realizations, seen numerically in chapter six, there is an accurate determination of the group delay of the unknown optical pulse. While it is also seen in chapter six that the accuracy of determining the group delay is dependent on both the total number of realizations and the discretization of the frequency to spatial conversion, only one diagonal of the mask matrix was used. All other diagonals with the same sign could be used to decrease the total number of realizations needed for a given amount of accuracy. This additional information stems from the fact that all other diagonals, with the same sign, contain different frequency mixing which all originate from the same unknown optical pulse.

References

[1]   T. Maiman, "Stimulated Optical Radiation in Ruby," Nature (London) 187, 493 (1960)

[2]   Lengyel, Bela A. (1962). *Lasers: Generation of Light by Simulated Emission*. John Wiley & Sons. pp. 22–28.

[3]   Townes, Charles H. (2003). Laura Garwin and Tim Lincoln (ed.). "The First Laser". *A Century of Nature: Twenty-One Discoveries that Changed Science and the World*. University of Chicago Press. pp. 107–12.

[4]   A. Javan, "Possibility of Production of Negative Temperature in Gas Discharges," Phys. Rev. Lett. 3, 87 (1959)

[5]   Basov, N. & Zuev, V. & Senatsky, Yury. (1965). Neodymium-glass laser with pulsed Q switching. JETP letters. 2. 35.

[6]   W. Filensky and H. -. Klein, "The GaAs MESFET as a Pulse Regenerator, Amplifier and Laser Modulator in the Gbit/s Range," *ESSCIRC 76: 2nd European Solid State Circuits Conference*, 1976, pp. 90-91, doi: 10.1109/ESSCIRC.1976.5469079.

[7]   D. Bradley, M. Holbrook and W. Sleat, "Bandwidth-limited picosecond pulses from an actively mode-locked GaAlAs diode laser," in *IEEE Journal of Quantum Electronics*, vol. 17, no. 5, pp. 658-662, May 1981, doi: 10.1109/JQE.1981.1071193.

[8]   Y. Silberberg and P. Smith, "Subpicosecond pulses from a mode-locked semiconductor laser," in *IEEE Journal of Quantum Electronics*, vol. 22, no. 6, pp. 759-761, June 1986, doi: 10.1109/JQE.1986.1073067.

[9]   M. Yoshizawa and T. Kobayashi, "Experimental and theoretical studies on colliding pulse mode locking," in *IEEE Journal of Quantum Electronics*, vol. 20, no. 7, pp. 797-803, July 1984, doi: 10.1109/JQE.1984.1072475.

[10]   J. A. R. Williams, P. M. W. French and J. R. Taylor, "An investigation into femtosecond pulse formation in a continuously-pumped passively-mode-locked CPM ring dye laser," in *IEEE Journal of Quantum Electronics*, vol. 26, no. 8, pp. 1434-1439, Aug. 1990, doi: 10.1109/3.59693.

[11]   J. Murray, "Temporal compression of mode-locked pulses for laser-fusion diagnostics," in *IEEE Journal of Quantum Electronics*, vol. 17, no. 9, pp. 1713-1723, September 1981, doi: 10.1109/JQE.1981.1071315.

[12]   T. Kobayashi, H. Yao, K. Amano, Y. Fukushima, A. Morimoto and T. Sueta, "Optical pulse compression using high-frequency electrooptic phase modulation," in *IEEE Journal of Quantum Electronics*, vol. 24, no. 2, pp. 382-387, Feb. 1988, doi: 10.1109/3.135.

[13]   J. A. R. Williams, P. M. W. French and J. R. Taylor, "An investigation into femtosecond pulse formation in a continuously-pumped passively-mode-locked CPM ring dye laser,"

in *IEEE Journal of Quantum Electronics,* vol. 26, no. 8, pp. 1434-1439, Aug. 1990, doi: 10.1109/3.59693.

[14]   D. J. Kane and R. Trebino, "Characterization of arbitrary femtosecond pulses using frequency-resolved optical gating," in IEEE Journal of Quantum Electronics, vol. 29, no. 2, pp. 571-579, Feb. 1993, doi: 10.1109/3.199311.

[15]   D. J. Kane and R. Trebino, "Single-shot measurement of the intensity and phase of an arbitrary ultrashort pulse by using frequency-resolved optical gating," in Optical Letters, vol. 18, issue 10, pp. 23-25, 1993.

[16]   K. W. DeLong, R. Trebino, J. Hunter and W. E. White, "Frequency-resolved optical gating with the use of second-harmonic generation," in Journal of the Optical Society of America B, vol. 11, issue 11, pp. 2206-2215, 1994.

[17]   M. Takeda, J. Ina, and S. Kobayashi, "Fourier-transform method of fringe-pattern analysis for computer-based topography and interferometry," in Journal of the Optical Society of America, vol. 72, issue 1, pp. 156-190, 1982.

[18]   M. Dantus, V. V. Lozoovoy, and I. Pastirk, "Measurement and Repair: The femtosecond Wheatstone Bridge," in Optical Electronics 2003.

[19]   V. V. Lozovoy, I. Pastric, and M. Dantus, "Multiphoton intrapulse interference 4: Characterization and compensation of the spectral phase of ultrashort laser pulses," in Optics Letters, vol. 29, pp. 775-777, 2004.

[20]   B. Xu, J. M. Gunn, J. M. Dela Cruz, V. V. Lozovoy, and M. Dantus, "Quantitative investigation of the MIIPS method for phase measurement and compensation of femtosecond laser pulses," in Journal of Optical Society of America B, vol. 23, pp. 750-759, 2006.

[21]   M. J. Soileau, W. E. Williams, E. W. Van Stryland, T. F.Boggess, and A. L. Smirl, "Temporal dependence of laser-induced breakdown in NaCl and SiO2," in Laser-InducedDamage in Optical Materials: 1982, H. E. Bennett, A. H.Guenther, D. Milam, and B. E. Newnam, eds., Natl. Bur.Stand. (U.S.) Spec. Publ. 669, 387–405 (1984).

[22]   M. J. Soileau, W. E. Williams, E. W. Van Stryland, T. F.Boggess, and A. L. Smirl, "Temporal dependence of laser-induced breakdown in NaCl and SiO2," in Laser-InducedDamage in Optical Materials: 1982, H. E. Bennett, A. H.Guenther, D. Milam, and B. E. Newnam, eds., Natl. Bur.Stand. (U.S.) Spec. Publ. 669, 387–405 (1984).

[23]   E. S. Bliss, "Pulse duration dependence of laser damagemechanisms," Opto-Electronics 3, 99–108 (1971).

[24]   J. R. Bettis, R. A. House II, and A. H. Guenther, "Spotsize and pulse duration dependence of laser-induced dam-age," in Laser-Induced Damage in Optical Materials: 1976, A. J. Glass and A. H. Guenther, eds., Natl. Bur. Stand. Spec.Publ. 462, 338–345 (1976).

[25]   Stuart, B. & Feit, Michael & Herman, Sophia & Rubenchik, Alexander & Shore, Bruce & Perry, Michael. (1996). Optical ablation by high-power short-pulse lasers. JOSA B. 13. 459-468. 10.1364/JOSAB.13.000459.

[26]   Oliver Haupt, Dirk Muller and Frank Gabler "Shorter Pulse Widths Improve Micromachining," https://www.photonics.com/article.aspx?aid=54123.

[27]   B. E. A. Saleh, and M. C. Teich, Fundamental of Photonics. Second Edition, John Wiley & Sons, Inc. ISBN 978-0-471-35832-9, 2007.

[28]   R. W. Boyd, Nonlinear Optics. Second Edition, Academic Press, ISBN 978-0-12-121682-5, 2003.

[29]   G. Gallot and D. Grischkowsky, "Electro-optic detection of terahertz radiation." J. Opt. Soc. Am. B 16. (1999) 1204.

[30]   J. D. Jackson, *Classical Electrodynamics* (McGraw-Hill, New York 1975), 2nd ed., p. 739; W. K. H. Panofsky and M. Phillips, *Classical Electricity and Magnetism* (Addison-Wesley, Reading, Mass., 1962), p. 131.

[31]   L. D. Landau and E. M. Lifshitz, *Electrodynamics in Continuous Media* (Pergamon Press, New York, 1960), p. 252.

[32]   T. B. Pittman, Y. H. Shih, D. V. Strekalov, and A. V. Sergienko, "Optical imaging by means of two-photon quantum entanglement," Phys. Rev. A 52, R3429-R3432 (1995).

[33]   R. S. Bennink, S. J. Bentley, and R. W. Boyd, ""Two-photon" coincidence imaging with a classical source," Phys. Rev. Lett. 89, 113601 (2002).

[34]   M. D'Angelo and Y. Shih, "Can quantum imaging be classically simulated?," arXiv.org, arXiv:quant-ph0302146v2 (2003).

[35]   A. Gatti, E. Brambilla, and L. A. Lugiato, "Entangled imaging and wave particle duality: the microscopic to the macroscopic realm," Phys. Rev. Lett. 90, 133603 (2003).

[36]   R. S. Bennink, S. J. Bentley, R. W. Boyd, and J. C. Howell, "Quantum and classical coincidence imaging," Phys. Rev. Lett. 92, 033601 (2004).

[37]   A. Valencia, G. Scarcelli, M. D'Angelo, and Y. Shih, "Two-photon imaging with thermal light," Phys. Rev. Lett. 94, 183602 (2005).

[38]   F. Ferri, D. Magatti, A. Gatti, M. Bache, E. Brambilla, and L. A. Lugiato, "High-resolution ghost image and ghost diffraction experiments with thermal light," Phys. Lett. 94, 183602 (2005).

[39]   A. Gatti, E. Brambilla, M. Bache, and L. A. Lugiato, "Correlated imaging, quantum and classical," Phys. Rev. A 70 013802 (2004).

[40] A. Gatti, E. Brambilla, M. Bache, and L. A. Lugiato, "Ghost imaging with thermal light: comparing entanglement and classical correlation," Phys. Rev. Lett 93. 093602 (2004).

[41] Y. Cai and S.-Y. Zhu, "Ghost imaging with incoherent and partially coherent light radiation," Phys. Rev. E 71 056607 (2005).

[42] Y. Cai and S.-Y. Zhu, "Ghost interference with partially coherent light radiation," Opt. Lett. 29, 2716-2718 (2004).

[43] G. Scarcelli. V. Berardi, and Y. Shih, "Can two-photon correlation of chaotic light be considered as correlation of intensity fluctuations?" Phys. Rev. Lett. 96, 063602 (2006).

[44] B. I. Erkmen, and J. H. Shapiro, "Unified theory of ghost imaging with Gaussian-state light," Phys. Rev. A 77, 043809 (2008).

[45] L. Basano and P. Ottonello, "A conceptual experiment on single-beam coincidence detection with pseudothermal light," Opt. Express 19, 12386-12394 (2009).

[46] J. H. Shapiro, "Computational ghost imaging," Phys. Rev. A 78, 061802(R) (2008).

[47] Isserlis, L. "On a formula for the product-moment coefficient of any order of a normal frequency distribution in any number of variables." Biometrika. 12 (1–2): 134–139 (1918).

[48] J. W. Goodman, "Some fundamental properties of speckle*," J. Opt. Soc. Am., 66, 1145-1150 (1976).

[49] J. W. Strutt (Lord Rayleigh), "On the resultant of a large number of vibrations of the same pitch and of arbitrary phase," Philos. Mag., 10, 73-78 (1880).

[50] K. Pearson, A Mathematical Theory of Random migration (Draper's Company Research Memoirs, London, 1906), Biometric Ser. III.

[51] J. W. Strutt (Lord Rayleigh), "On the problem of random vibrations, and of random flights in one, two, or three dimensions," Philos. Mag., 37, 321-347 (1919).

[52] J. W. Goodman, "Statistical properties of laser speckle patterns," Laser Speckle and Related Phenomena (Topics in Applied Physics), 9, 9-75 (1975).

[53] Hughes-Hallet, Gleason, McCallum et al. Calculus Single and Multivariable, Second Edition, John Wiley & Sons, Inc., SIBN 0-471-19490-5, 1998.

[54] J. V. Michalowicz, J. M. Nichols, F. Bucholtz, and C. C. Olson, "A general Isserlis theorem for mixed-Gaussian random variables," Stat. Prob. Lett 81, 1233-1240 (2011).

[55] O. E. Martinez, Journal of optical Society of America B, vol. 3, 929, 1986.

[56] M. van Exter, Ch. Fattinger and D. Grischkowsky, "High Brightness TeraHz Beams Characterized with an Ultrafst Detector," Appl. Phys. Lett. vol. 55, pp. 337-339, 1989.

[57] T. Tanabe, K. Suto, J. Nishizawa, K. Sato, and T. Kimura, "Tunable terahertz wave generation in the 3- to 7- THz region from GaP.," Appl. Phys. Lett., 83, pp 237-239, 2003.

[58] DLP650LNIR 0.65 NIR WXGA S450 DMD, www.ti.com/product/DLP650LNIR#product-details, DLPS136- August 2021.

[59] Near-IR Ruled Reflective Diffraction Gratings, www.thorlabs.com/newgrouppage9.cfm?objectgroup_id=8627- August 2021.

[60] W. H. Press, W. T. Vetterling, and S. A. Teukolsky, Numerical Recipes in C, 2nd ed. Cambridge, U.K.: Cambridge Univ. Press, 1992.

[61] K. W. Delong, D. N. Fittinghoff, and R. Trebino, "Practical Issues in Ultrashort-Laser-Pulse Measurement Using Frequency-Resolved Optical Gating," IEEE Journal of Quantum Electronics, Vol 32 No. 7 1253 (1996).

[62] Rick Trebino, Frequency-Resolved Optical Gating: The Measurement of Ultrashort Laser Pulses, Springer Science+Buisiness Media ISBN 978-1-4613-5432-1 2000.

[63] F. Stibenz and G. Steinmeyer. "Optimizing spectral phase interferometry for direct electric-field reconstruction," Review of Scientific Instruments, 77, 073105 (2006).

[64] B. Xu, J. M. Gunn, J. M. Dela Cruz, V. V. Lozovoy, and M. Dantus. "Quantitative investigation of the multiphoton intrapulse interference phase scan method for simultaneous phase measurement and compensation of femtosecond laser pulses," J. Opt. Soc. Am. B Vol. 23 No. 4 2006.